STUDIES IN BIOLOGICAL SURFACE SCIENCE: MICROFLUIDICS,

PHOTOPATTERNING AND ARTIFICIAL BILAYERS

A Dissertation

by

MATTHEW ALEXANDER HOLDEN

Submitted to the Office of Graduate Studies of
Texas A&M University
in partial fulfillment of the requirements for the degree of

DOCTOR OF PHILOSOPHY

May 2004

Major Subject: Chemistry

STUDIES IN BIOLOGICAL SURFACE SCIENCE: MICROFLUIDICS,

PHOTOPATTERNING AND ARTIFICIAL BILAYERS

A Dissertation

by

MATTHEW ALEXANDER HOLDEN

Submitted to Texas A&M University
in partial fulfillment of the requirements
for the degree of

DOCTOR OF PHILOSOPHY

Approved as to style and content by:

Paul S. Cremer	Ali Beskok
(Chair of Committee)	(Member)

Gyula Vigh	Richard M. Crooks
(Member)	(Member)

Emile A. Schweikert
(Head of Department)

May 2004

Major Subject: Chemistry

ABSTRACT

Studies in Biological Surface Science: Microfluidics, Photopatterning and Artificial

Bilayers.

(May 2004)

Matthew Alexander Holden,

B.S., University of Florida

Chair of Advisory Committee: Dr. Paul S. Cremer

Herein is presented the collective experimental record of research performed in the Laboratory for Biological Surface Science. These investigations are generally classified under the category of bioanalytical surface science and include the following projects. Chapters III and IV describe the creation of a microfluidic device capable of generating fixed arrays of concentration gradients. Experimental results were matched with computational fluid dynamics simulations to predict analyte distributions in these systems. Chapters V and VI demonstrate the discovery and utility of photobleaching fluorophores for micropatterning applications. Bleached fluorophores were found to rapidly attach to electron rich surfaces and this property was used to pattern enzymes inside microfluidic channels *in situ*. Finally, Chapter VII exhibits a method by which solid supported lipid bilayers can be dried and preserved by specifically bound proteins. The intrinsic property of lateral lipid mobility was maintained during this process and a mechanism by which the protein protects the bilayer was suggested.

ACKNOWLEDGMENTS

This dissertation attests to the fact that I conducted scientific research and then wrote a dissertation about the research I conducted. However, it tells no more. The reader will find no record of my triumph or despair, which both accompanied me during my four years. Although the following pages detail proud breakthroughs made in the Laboratory for Biological Surface Science, my greatest discoveries were the friends I met here. So that this dissertation will not be grossly incomplete, I take this opportunity to extend my most sincere gratitude towards to them.

I first thank my advisor Paul, whose guidance through the dark times and confidence in my ability spurred me on when I met with doubt. You always thought I would succeed, and once again, you were correct. Next, I thank the Superjung, who I shared my struggle with for so long. I struggle once more to describe our friendship; I can only say that "best" is not an adequate descriptor. Spasiba to Olitchka, I wish you could've been here all along. I put my poetry into *JACS*. Tinglu, you were a never-ending source of courage and wisdom, and I can't thank you enough for all your time and help. Fernando, your energy and enthusiasm is beyond description. Your mere presence is an inspiration to us all. Chairman Mao, you showed us all about finishing. To Ed, Marc, Soon, Sho and the Cremer Group, there's really only one thing to say: I couldn't have done this without you.

Many thanks to Gyula Vigh, Dick Crooks and Ali Beskok, my graduate committee. I greatly appreciate the time you've taken to guide me through my prelim and defense and for all the helpful advice you've given me. Thank you once again for your help with

this dissertation.

I'd also like to thank Saurabh Kumar, my fellow collaborator from mechanical engineering. Together, we spent nearly two years struggling to bridge the gap between experiment and theoretical simulation. We produced two papers on the subject, but tragically, you never got to see them in print. When I learned the sad news that you'd passed away, I contacted the editors of both journals and had the works dedicated to your memory. It was the least I could do for such an outstanding friend and colleague.

Finally, I thank my mom Char and my dad Phil. Despite the distance, you've stayed close at heart and have been an inexhaustible source of support. This dissertation marks the end of being a student, which I know the two of you have been waiting to see for a long time. But, as the cliché goes, this end leads to a beginning. When I reflect on the journey between my childhood and today, I can't help but to be in awe of my tremendous fortune to have such amazingly cool parents. Thank you for everything, I love you both very much.

TABLE OF CONTENTS

LIST OF FIGURES

CHAPTER I

INTRODUCTION

The fields of biology and surface science once existed as separate worlds. In recent years, however, these areas have come together to create a new type of interdisciplinary research -- biological surface science.[1-3] The fundamental mantra of this expanding field is understanding the interface. The way in which viruses recognize cell surfaces,[4,5] proteins adhere nonspecifically to various materials,[6] or chemical inputs travel from cell to cell[7,8] are but a few of the subdivisions of biological surface science. Although the research of this dissertation was motivated by these themes, the experimental approach was borne from the perspective of analytical chemistry. Thus, the material presented here centers on novel methodology, which has the potential to enhance our ability to observe biological surface phenomena. The experiments and results which follow detail these developments, and are divided into the following Chapters.

Chapter II provides an overview of several procedures and useful tips which were crucial to the development of the experimental methods.

Chapter III focuses on the development of a microfluidic geometry which enables the creation of a universal concentration gradient. Microfluidic technology has become a cornerstone of modern analytical chemistry. The reduction of traditional bench top chemistry to the micrometer scale has provided researchers with several key advantages, including low sample volume, high surface area to volume ratios and parallel analysis.

This dissertation follows the format and style of *Journal of the American Chemical Society.*

More importantly, fluids moving in microchannels almost always flow laminarly, not turbulently as in bench top processes. Therefore, relating quantitative properties, such as flux to reaction kinetics, is more straightforward.

This laminar behavior[9-12] was employed to create concentration gradients using parallel flowing streams. When combined at a Y junction, two streams will flow side by side, rather than mixing by turbulence, when the Reynolds number (the quantitative descriptor of turbulence) is far below 2000. Instead, molecules in these streams interdiffuse in a predictable manner. The subject of Chapter III describes how this fundamental microfluidic property was used to create the microfluidic diffusion diluter, which forms discrete concentration gradients which could be used combinatorially for concentration dependent measurements. This device was fabricated from glass to form a completely rigid device, thus preventing channel deformation during pressure-driven flow.

Chapter IV continues the study of the microfluidic diffusion diluter, however this device was fabricated from a hybrid PDMS/glass system.[13] Since PDMS is a flexible polymer, devices made using this fast and simple method undergo channel geometry changes during flow. Here, data are presented which show channel bulging in all areas of the device, and that this bulging was dependent on the flow rate.

Chapter V describes a novel method by which photobleaching fluorophores can lead to direct covalent surface attachment of proteins and ligands. This research shares its relation to biological surface science through its potential for improving array-based technologies.[14-16] Both DNA and protein arrays have become increasingly popular in the

last 5 years. The vast majority of such arrays are created by simple mechanical printing using robotically controlled pins.[17,18] Nanoliter sized drops of DNA fragments or protein or peptide sequences are arranged in square grids over which solutions of target molecules can be introduced and binding detected. Typically, these plates are dried, therefore many samples either lose some biological activity or are unsuitable altogether. Also, this technique is plagued by low spatial resolution and spot density, as drops tend to spread. Inkjet deposition of proteins and DNA has similar drawbacks.[19] Photolithographic approaches[20] to array generation can avoid such issues, and yield higher density samples. There are, however, unique disadvantages to this and similar systems as well. Always, the irradiation comes from a UV source, which is a potentially damaging form of radiation. Also, several methods require harsh organic solvents, which would denature more delicate protein structures.

Fluorescent dyes all suffer from a tendency to photobleach. While typically this is an undesired effect, Chapter V describes the discovery of an unexpected and practical application. When a fluorophore bleaches, the fluorescence is generally shifted far to the blue, and thus invisible to the same filter set used for bleaching. However, what happens to the bleached species is often ignored. This research section shows that the fluorophore becomes highly reactive in its bleached state, which follows an oxygen dependent pathway. Upon activation, bleached fluorophores seek out sites of electron density, which can be in the form of the amino acid side chains of a sacrificial protein monolayer. Using ligand-linked dyes or dyes directly attached to proteins, patterns of proteins can be formed by high power laser irradiation at the fluorophore's resonance. In

this case, visible light is used for patterning a key advance over UV patterning. However, the greatest benefit, derives from the complete aqueous compatibility of the entire process from start to finish, which makes it quite protein friendly. Overall, this method provides an attractive alternative to previous photopatterned protein arrays.

Chapter VI demonstrates a powerful example of the utility of the fluorophore bleaching immobilization method. Here, a ligand linked dye, biotin-4-fluorescein was bleached to form patches of biotin inside PDMS microfluidic channels coated with a passivating protein layer. Once avidin or streptavidin linked enzymes were immobilized at the site of the biotin patches, substrate was infused and turnover observed via fluorogenic substrate cleavage.

Chapter VII explores a new method for the protection of solid supported lipid bilayers by specifically bound protein monolayers. The lipids in the membranes of living cells vary greatly in chemical nature, percent composition and physiological function. However, keeping cells alive during the study of biological surface phenomena requires painstaking care. Unfortunately, many conditions of pH, ionic strength, temperature and analyte concentration are beyond the viable range for cells, and therefore excluded experimentally. Artificial lipid bilayers provide an alternate route which greatly simplifies surface study.[21] Lipid vesicles, containing tailored amounts of phosphocholines, ceramides, sphingolipids, cholesterol and synthetic lipids can be easily created in solution without concern for cell viability, while still being biologically relevant. When brought into contact with a hydrophilic surface, vesicles spontaneously fuse to form continuous planar lipid bilayers. These systems have been

used to study biological surface phenomena such as ligand-receptor thermodynamics, lipid rafts and more.

Supported bilayers are destroyed when drawn through the air/water interface.[22] Research has been conducted to create air stable bilayers via polymerization cross-linking of lipids,[23] hybrid SAM/phospholipid bilayers[24] and forming bilayers on chemically modifies surfaces.[25] This bottom-up approach has led to bilayers which are less mobile or not mobile at all. However, little research about protecting bilayers from the topside has been done. Chapter VII shows that specifically bound proteins render bilayers impervious to the air/water interface. Where an unprotected bilayer pops open immediately upon removal from water, protein coated bilayers tenaciously hold water to the surface. The stability imparted by the protein stems from two properties. First, hydrophilic proteins trap water in a thin layer between the protein and bilayer. Second, the protective property of the protein works best when the surface is saturated. These close packed proteins prevent curling of the bilayer at the edges by stiffening the bilayer's bending elastic modulus. Such bilayers show the potential for long term storage and rehydration for future use.

CHAPTER II

EXPERIMENTAL AND INSTRUMENTAL BACKGROUND

PDMS/Glass Microfluidic Fabrication

The fabrication of PDMS microfluidics in our laboratory has undergone many stages of development in the lab during the last 4 years. The material presented in this section represents the most optimized procedures.

Beginning with the cleanest possible surface is one of the fundamental keys to high resolution, reproducible photolithography. Although other surfaces are more commonly used as substrates for photoresist, such as silicon and metals deposited on silicon, microscope slides have proven to be easy to clean and spincoat, and are vastly cheaper than silicon wafers. Corning provides 75 x 50 mm soda lime float glass slides which are ideally suited to the process described below. Generally, slides are boiled in a mild detergent solution of 7X (ICN Biomedical) in water for 30 minutes. The slides are removed using custom racks designed by Edward Castellana (Cremer Research Group) and thoroughly rinsed in house distilled water. Since some detergent sticks to the glass surface, slides are boiled again in pure water for 20 minutes and dried under a stream of nitrogen. Although slides cleaned this way can be stored in a tightly sealed box, freshly cleaned slides were usually immediately spin coated with photoresist and then stored.

Shipley S1813 is a low viscosity positive photoresist (Shipley, Marlborogh, MA) which spins to a thickness ranging from 5 to 10 microns at spin speeds between 150 and 200 RPM. Clean slides were attached to a glass vial with double-sided tape and the outer face of the glass was brought just into contact with a pool of photoresist. Slides

were then inverted, the glass vial removed, attached to a homemade spinner (an AC motor controlled with a Variac) with double sided tape and spun for 30 seconds. Though the manufacturer generally recommends hotplates for baking photoresist, the setup used for all research hereafter was a simple toaster oven controlled by a Variac. This oven was set to 90 degrees C and photoresist baked for 40 min. Finished slides were stored in total darkness until use.

The need for cleanroom conditions during the coating and development process was dictated by the size of the features to be patterned and the size of the overall pattern. Large patterns with small features (less than 5 microns) are not easily patterned using this method, as any particle of dust can cause a break in the continuous form. The sizes of the patterns presented here were tolerant enough to perform most procedures in a dust free laminar flow hood, rather than a clean room.

Photographic film negatives were used as contact photomasks for the majority of microfluidic patterning. Technical Pan film from Kodak is a high-resolution aerial photography film ideally suited for micropatterning. Using a bulk film loader, short sections of film could be exposed and developed rather than making masks one roll at a time. Patterns for microfluidics were created in CorelDraw 9 and printed on Epson PhotoQuality Inkjet paper using a Phaser 4200 printer at the best resolution (1200 dpi). Patterns had to be printed as a negative of the desired pattern. For example, white areas on paper became black on film, and black areas became clear film. To reduce the amount of black ink used, negative patterns were created with black borders, rather than a pattern in a large black area. This printed pattern was cut out and placed atop a piece

of black velvet, which reflects the least amount of light. The set up for mask making is shown in Figure 1. The height of the camera was adjustable for controlling the reduction amount. At its lowest setting, the reduction factor was 7.8, and this was used for most masks.

The camera used was an all manual control Pentax K1000 with a 50 mm lens. Through trial and error, an f-stop of 8 and an exposure time of 1/8 second were found to produced the sharpest features. The shutter speed was set to the slowest setting, but does not matter since the image doesn't move. Film had to be loaded onto development reels in complete darkness, and was then loaded into a small developing tank. It was developed for 7 minutes using Kodak D-19 developer, which comes as a pouch to be dissolved in pure water. After 30 seconds of stop bath, film was fixed with Kodak's generic fixer for 3 minutes. All solutions were reusable and generally lasted 6 months before losing efficacy. At this point, film could be exposed to room light, and was rinsed with pure water and dried with nitrogen. Any scratches in the film over the pattern rendered those images useless, as scratches scatter light during photoresist exposure.

Patterns were best made two at a time by taking the best two film masks and fixing them to a clean 75 x 50 mm slide with double sided tape. A sandwich of glass-film-photoresist-glass was clamped together with small binder clips (to ensure the mask made contact with the photoresist) and placed on the exposure stage of a Quintel 4000 mask aligner. Normally, this instrument is used for exposing 3-inch diameter wafers of
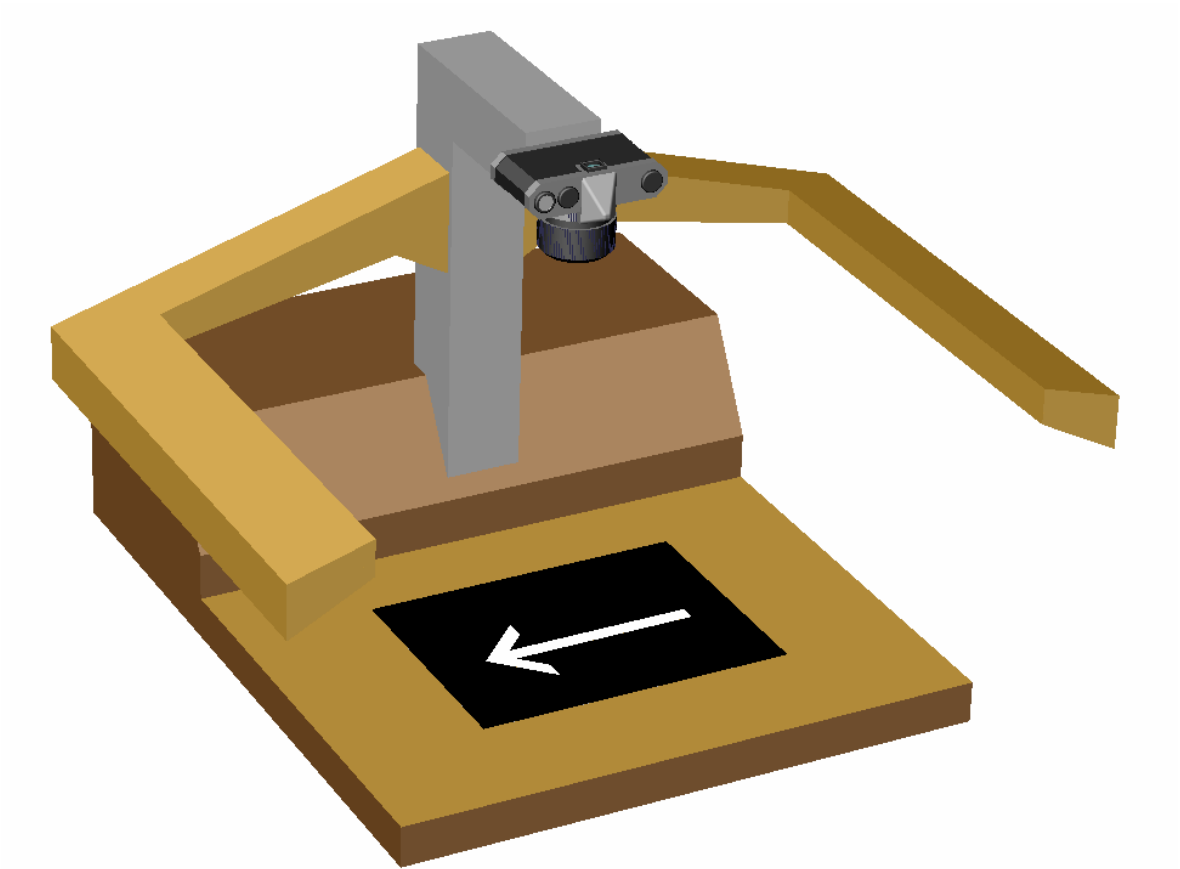
Figure 1. Mask making apparatus. This device was created by retrofitting a Pentax camera onto a microfiche recording platform. The pattern, in this case an arrow, is printed as a negative. Depending on the camera height, which was adjustable, reductions from 7.8 to 12 X was possible. To save on printer ink, patterns were often printed with a black border, cut out and placed on a surface of black velvet. Due to spherical aberrations, the finest features of new designs were placed as close to the center of the pattern as possible, since the camera had the highest fidelity at the center.

silicon, however, the corners of the 75 x 50 mm slide reached the edge of the unloaded stage platform, providing a level surface for mounting. Exposure times varied due to the lifetime loss of intensity of the illumination source. Therefore, the optimized exposure had to be determined each time. However, an exposure time of 70 seconds nearly always produced excellent patters and was the best starting point for optimization. Although the film appeared black in the patterned areas, some light leaked through, and longer exposure times lead to partial exposure of protected photoresist, resulting in a rough surface. This effect was clearly visible upon inspection with a light microscope. Too little exposure resulted in incomplete development.

Figure 2 outlines the overall photolithographic process. Exposed slides are developed in Microposit developer (Shipley) mixed equally with water for 30 seconds. Remaining areas of undesired photoresist are removed with a Kimwipe dabbed in acetone. Glass barriers were glued together from sections of microscope slides and fixed around the pattern with Krazy Glue (Elmer). PDMS monomer and crosslinker were mixed 10:1 by stirring and then degassed with a roughing vacuum. When all bubbles were removed, 6 grams of PDMS prepolymer was poured onto each pattern. Though there are myriad published ways to cure the PDMS prepolymer, the following procedure has been the most reliable. PDMS was cured on the benchtop overnight. The next morning, devices were placed into a 90 degree C oven for an hour. Devices were then peeled away from the photoresist mold (the mold is reusable) and inlet holes reamed with a hollow flat-tipped needle. The reamed holes were rinsed with a strong jet of DI water to remove small particles of PDMS which could clog smaller sections. The device

UV Source

Photomask

Photoresist

**Developed
Photopattern**

**Pour
PDMS**
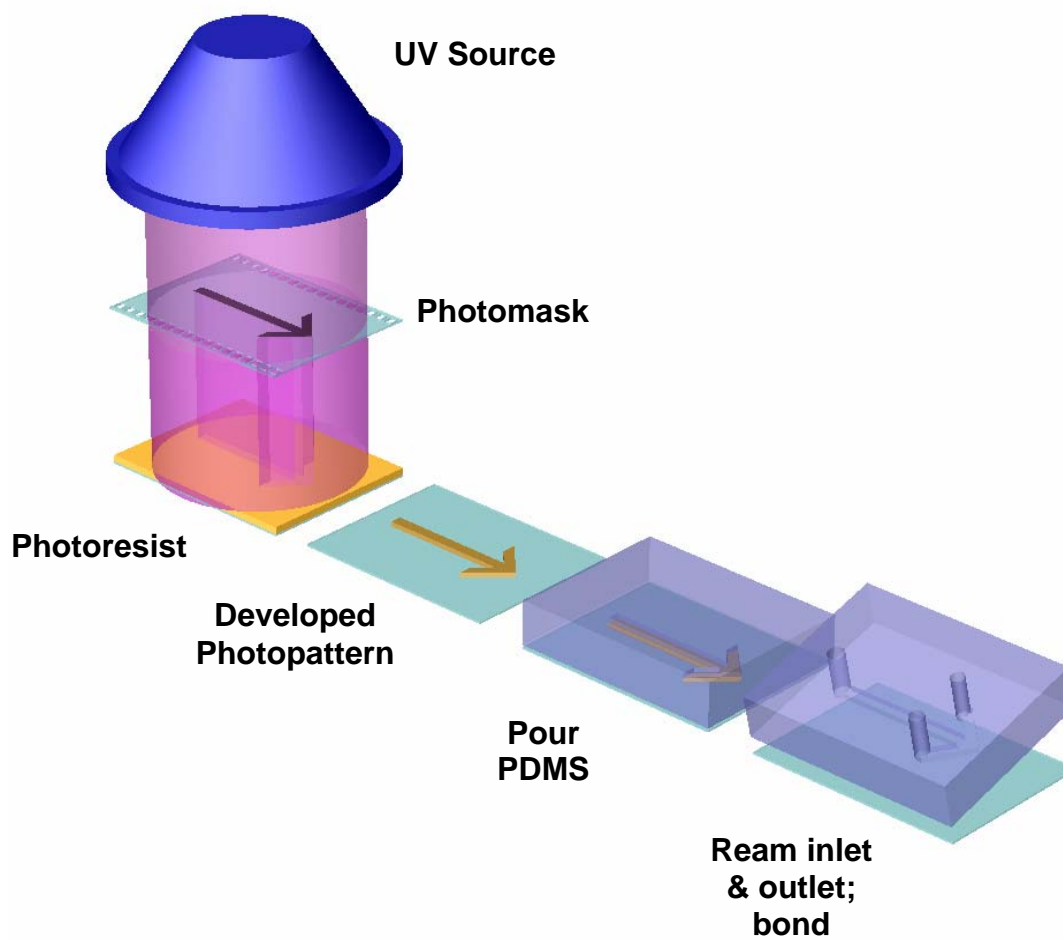
**Ream inlet
& outlet;
bond**

Figure 2. Photolithographic process. In practice, the film photomask actually touches the photoresist during exposure. Here, it has been offset for visual clarity. During plasma bonding, the stamp is usually inverted and the glass gently placed on top. This helps to prevent accidental bonding of the channel ceiling to the glass.

was then dried with a stream of nitrogen and placed into a plasma cleaner along with a clean, annealed 50 x 25 mm microscope cover slip. After 20 seconds of air plasma, the PDMS and glass were immediately brought into contact and an irreversible bond formed. To maintain channel hydrophilicity, water was injected into the inlet.

Glass Microfluidics

Though PDMS is a fast, cheap and easy microfabrication method, PDMS itself has some undesirable properties. PDMS is a flexible polymer, and therefore bulges during pressure-driven flow. Also, PDMS absorbs organic solvents rapidly, rendering organic chemistry incompatible without extensive surface modification. Glass on glass microfluidics avoids these issues, but is much more time consuming.

Identical procedures were used for cleaning and coating microscope slides with photoresist as with PDMS/glass devices. However, the photomask was reversed, so that only the areas requiring chemical etching were removed from the coated slide. Slides were etched and bonded using a process adapted from Lin and coworkers.[26] Before etching, the backsides of the glass slides were protected with acrylic tape. Photopatterned slides were gently wafted by hand in a BOE (buffer oxide etchant) solution (1:6 ratio of 48% HF:200 g NH_4F in 300 mL DI water) for 2.5 - 3 minutes and washed in a 1 M HCl solution for 20 min. Inlet holes 1 mm in diameter were drilled into the glass using a diamond coated drill bit (Wale Apparatus). A 25×37.5 mm planar soda-lime glass slide section was used as a cover for the channel system. Covers and etched chips were cleaned by boiling in 7X detergent and then placed in a warm 6:1:1 DI water:HCl:H_2O_2 solution for 5 minutes, a warm 5:1:1 H_2O:NH_4OH:H_2O_2 solution for 5

minutes, rinsed with copious DI water and dried with N_2. Devices were bonded by stacking the plates between weights in the following order: 0.5" thick solid brass substrate (which served as a base), a polished alumina flat, the etched chip (channels up), a soda-lime cover, a second smaller polished alumina flat, and finally a 40 g brass weight. During thermal bonding, the weight would press on the alumina flat causing the two glass surfaces to fuse. After a first firing, the weight and the flat would be moved to an unbonded section and the firing schedule rerun. This process was repeated until all vital areas were bonded. The firing sequence was as follows: from room temperature a 280 ºC/hr ramp was applied up to 400 ºC and held at that temperature for 4 hours. Next, a 280 ºC/hr ramp was applied up to 588 ºC and held for 6 hours. Finally, the kiln was shut off and allowed to cool back to ambient temperature overnight.

Dealing with Bubbles

Interfacing macroscopic instruments with microfabricated systems presents perhaps the greatest engineering challenge in microfluidics. Of primary interest was infusing samples into microfluidic channels without the introduction of air bubbles. In the case of both PDMS and glass devices, a simple method was developed to handle this issue. Typically, solutions were injected by syringes mounted on a syringe pump. Each syringe had a custom fitting which allowed the attachment of a flexible plastic flow line. Therefore, the first step was to ensure no bubbles were allowed into the syringe/line system. The flexible line was dipped into a small vial of the solution to be filled, and the plunger of the syringe pulled all the way out, such that fluid in the vial siphoned into the barrel of the syringe. When a drop hung from the end of the syringe barrel, the plunger

was pushed back in about half way. The syringe was then mounted to the syringe pump.

To fill the syringe completely, a small portion of solution was pushed out of the inlet line

into the vial, and then the plunger was pulled all the way back to the syringe pump

pusher block with the line still in the vial. PDMS devices are particularly simple,

because the inlet line could be pushed directly into the inlet hole. In this case, the end of

the line was cut at an oblique angle. To ensure no bubbles were in the device itself, a 1

mL syringe with a needle attached was used to force a jet of water or buffer into each

inlet. Since the needle was smaller than the diameter of the outlet, the water shot back

out bringing trapped air out as well. Before plugging the line into the device, the

needled syringe was used to create a small dome of water over the inlet. Also, a small

drop was pushed from the inlet line using the pump and the two domes of water were

brought together when the line was finally inserted into the inlet. The same was true of

the all glass system, with the exception of the adapter which held the glass chip. This is

discussed in Chapter III.

Photobleach Micropatterning

The bleaching of a fluorophore depends on its quantum efficiency, excitation

wavelength and input power, and dissolved oxygen concentration. Typically, a high

quantum efficiency fluorophore is designed such that radiative decay is the most likely

relaxation process. Photobleaching, by contrast, is generally an undesired event, since

the fluorophore is no longer visible at its normal emission wavelength. However, as

Chapter V will demonstrate, fluorophores can become highly reactive just after

photobleaching, leading to a novel strategy for photoattachment chemistry.

Several fluorophores were tested during the first trials of photobleach micropatterning. Alexa594, Alexa488, Texas Red (Molecular Probes) and fluorescein all patterned during excessive irradiation, although to different extents based on the parameters described above. Fluorescein, by far, bleached the fastest of all tested species, and therefore became the molecule of choice for most patterning experiments. Most initial bleaching experiments were conducted using the excitation light from a Nikon E800 microscope. However, the vast majority of photobleaching was done using a more powerful Ar^+/Kr^+ continuous wave laser. Figure 3 shows the experimental setup for laser photobleaching.

Rather than focusing the laser on a particular channel or array before illumination, the microchannels were scanned across the laser using a syringe pump turned on its side. Attached to the pump pusher block was a Plexiglas arm which extends down to a platform onto which the device was placed. The inner block of the platform can move laterally by turning a small wheel. The lateral motion was used to photobleach multiple patterns inside microchannels at well defined intervals. When bleaching fluorescein, the laser was tuned to the 488 nm line at a power of 150 mW. The syringe pusher block could scan as fast as 2 mm per second, however, 1 mm per second was found to be sufficient to completely saturate the surface with bleached species. In other words, providing more illumination to each channel by scanning at a slower speed did not yield a greater patterning density.

The orientation of the chip on the platform was crucial to obtaining a single patterned patch per scan. A PDMS/glass chip has several interfaces between different
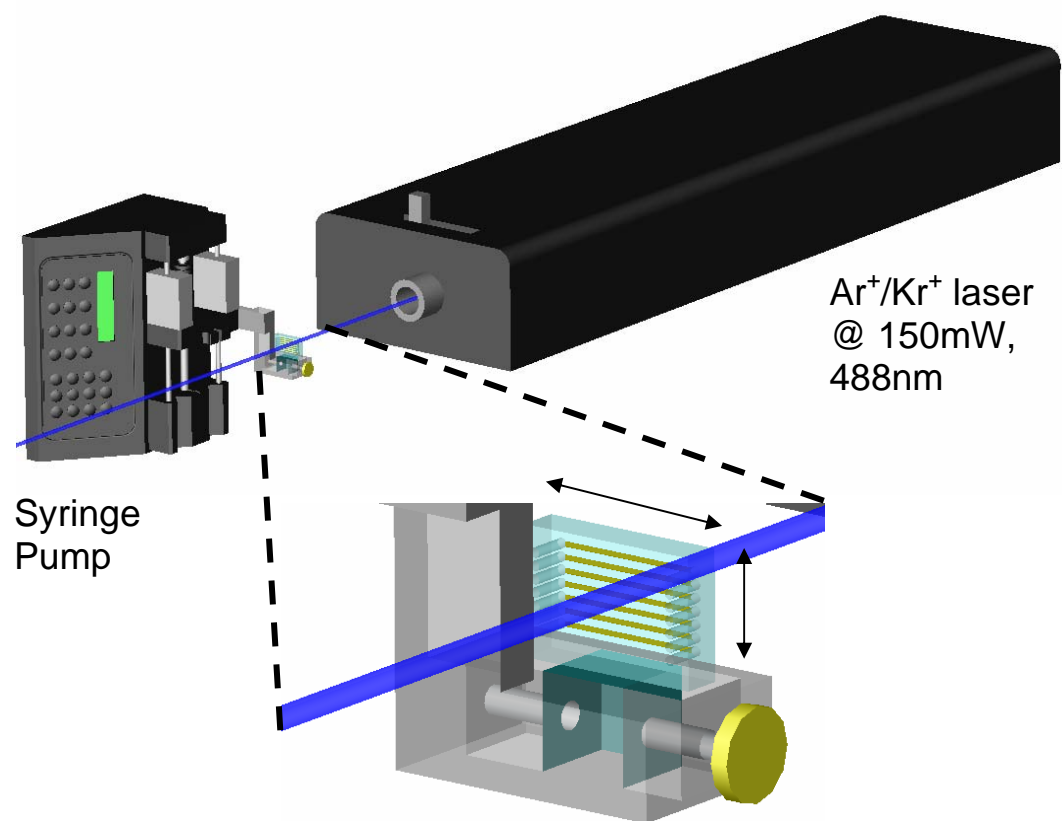
Figure 3. The laser photobleach micropatterning process. The channels of the PDMS/glass device are scanned vertically through the laser path using the motion of the pump, typically at 1mm/sec. The knob (yellow) can be turned to precisely move the stamp laterally for multiple patterns in the same channel. The knob turns a 0.080" threaded screw, such that 3 turns move about 1 mm. The dashed lines lead to a blowup showing the device itself. Note that the actual stamp rests on the movable block (blue).

media (air/glass, glass/PDMS, PDMS/air) and each interface can potentially reflect light back to the microchannel. It was therefore important to align the channel face as close to perpendicular to the laser path as possible, to prevent reflected light from also patterning.

CHAPTER III

GENERATING FIXED CONCENTRATION ARRAYS IN A MICROFLUIDIC

DEVICE*

Introduction

Microfluidic technology has attracted increasing interest over the last decade. The impetus behind recent advances such as microvalves,[27-31] surface modification,[32-37] unique geometries,[38,39] serial and parallel diluters,[40-42] as well as 3D lithography[43-45] has been the need to control the movement and mixing of minute quantities of fluids quickly and precisely at low Reynolds numbers. One particularly intriguing achievement was the development of the T-sensor [9,10,46] and similar devices.[11,12,23,47] This technique combines two flowing tributaries into a single stream and allows the contents to mix by diffusion as the liquids progress down the channel. Fluorescent tags or colorimetric changes can then be exploited to monitor analytes as a function of chemical or physical properties at any point along the diffusion gradient.

In the present work we exploit diffusional mixing inside a flowing stream as a first step in a procedure to permanently separate chemically distinct aqueous solutions into a series of parallel channels. We refer to this process as µDD. The purpose of this technique is to isolate arrays of analytes for (1) surface patterning, (2) heterogeneous assay development, and (3) the creation of multidimensional screens for combinatorial chemistry. The general concept is illustrated schematically in Fig. 4. Two streams of liquid are combined at a junction and allowed to diffuse into each other as they flow

Figure 4. (a) A schematic representation of μDD of two analytes into a series of parallel microchannels. (b) An epifluorescence micrograph of 23 parallel microchannels during the operation of the diffusion diluter device at a flow rate of 100 nL/min. (c) Line profiles of fluorescence intensity (arbitrary units) taken across the blue line in (b). The red curve shows the intensity of the Alexa 594 and the green curve is for Alexa 488. The microchannels spanned the entire 3.2 mm field of view of our microscope using a 4X objective.

downstream side by side. After a fixed distance, they are partitioned into a series of smaller channels that emanate from the main flow stream.   The shape of the concentration gradient formed by this process was studied as a function of flow rate using (1) experiments performed in glass microchips and (2) computational fluid dynamics simulations.

Theory

Analysis of Convective Diffusive Transport in Straight Channels. Incompressible fluid flow and convective/diffusive transport of a passively advected scalar field are governed by the (1) Navier-Stokes, (2) species transport, and (3) continuity equations:

$$\frac{\partial \vec{u}}{\partial t} + (\vec{u} \cdot \nabla)\vec{u} = -\nabla p + \frac{1}{Re}\nabla^2 \vec{u} \tag{1}$$

$$\frac{\partial \Theta}{\partial t} + \vec{u} \cdot \nabla \Theta = \frac{1}{Pe}\nabla^2 \Theta \tag{2}$$

$$\nabla \cdot \vec{u} = 0 \tag{3}$$

where $\vec{u}$ is the velocity vector, Θ is the normalized concentration density, p is the pressure, Re is the Reynolds number, and Pe is the Peclet number, based on the Schmidt number. The Reynolds number is defined as

$$Re = \frac{Uh}{\nu},$$

where $U,\ h$ and ν are the reference velocity, characteristic length and the kinematic viscosity, respectively. The Peclet number is defined as

$$Pe = \frac{Uh}{\alpha},$$

where α is the mass diffusivity. In equations (1-3) the velocity vector $\vec{u}$ is normalized using a reference velocity, U, and the concentration value, Θ is normalized using the analyte concentration at the inlet of the μDD. The pressure is normalized using the dynamic head (ρU^2).

Three Dimensional Velocity Field and Concentration Distribution. CFD-ACE+ (CFD Research Corporation, Huntsville, Alabama) was used to obtain three-dimensional velocity and concentration distributions in the main channel. Simulations were performed for a volumetric flow rate of 500 nL/min and normalized concentration values of Θ=0 and Θ=1 across half of the channel width, respectively. The channel width is 500 μm, while its height is ~6 μm; hence, the channel aspect ratio (width to height ratio) was ~90. For such large aspect ratios, mostly two-dimensional streamwise velocity (u) distribution is observed, as shown in Figure 5a. The streamwise velocity profile is mostly uniform in the spanwise direction (y), except very close to the side walls it decays to zero to comply with the no-slip boundary conditions. Streamwise velocity (u) variation is parabolic across the height of the channel (z-direction), typical of pressure-driven flows between two parallel plates. The velocity components along the y and z directions are negligible.

Concentration variations obtained from three-dimensional simulations are shown in Figure 5b. The concentration distribution on the lateral plane in the middle of the

channel is shown, as well as several vertical cross sections. Slight transverse diffusive

broadening is observed only very near the entry to the main channel.[48,49] Even at
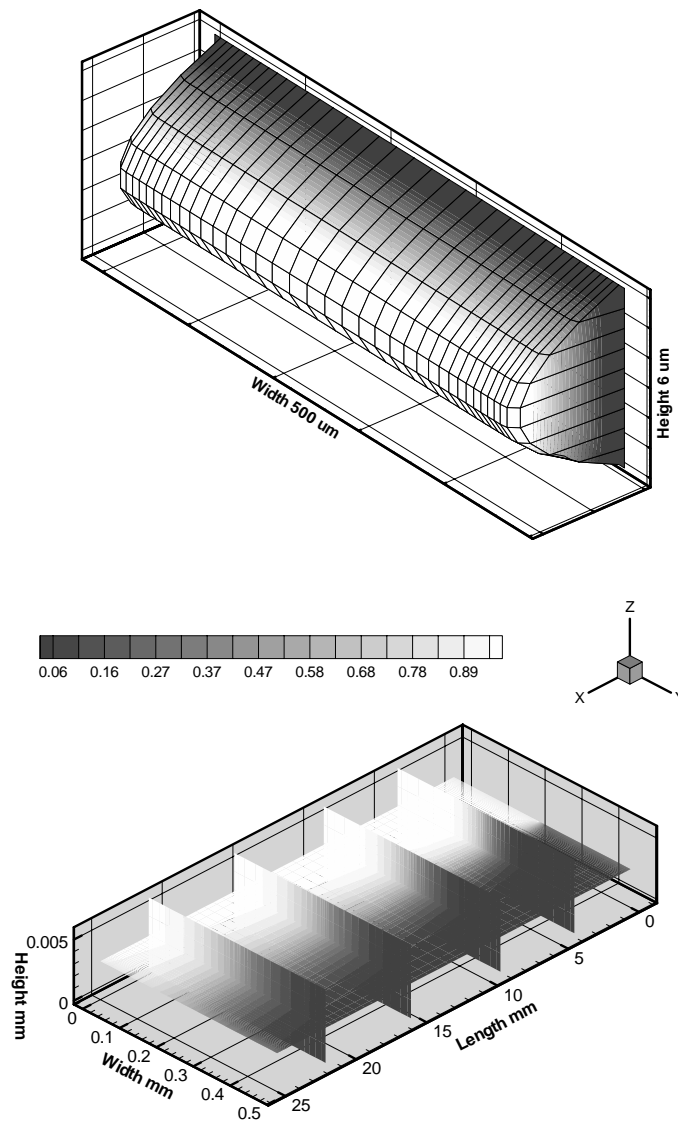

Figure 5. (a) Streamwise velocity distribution in a rectangular cross-section channel. Spanwise and cross-channel dimensions are not drawn to scale. (b) Concentration distribution in the main channel at various vertical sections.

small distances away from entry, the concentration contours shown in Figure 5b indicate no variations along the height of the channel. Therefore, diffusion mainly takes place along the streamwise and spanwise direction and the concentration profile can be assumed to be two-dimensional, and transverse diffusive broadening is negligible for high aspect ratio channels.[48,49]

Analytical Model for Concentration Distribution. Equations (1-3) can be simplified by assuming steady ($\partial \vec{u}/\partial t = 0$ and $\partial \Theta/\partial t = 0$), fully developed flow ($\partial \vec{u}/\partial x = 0$) conditions. The latter approximation is valid due to the simple geometry, where the flow development effects are confined to a very small portion of the channel inlet for small Reynolds number flows (in the present case: Re<1.389). In addition, the main velocity component is in the streamwise direction while the spanwise and cross flow velocity components are negligible (i.e., $\vec{u} \approx u e_x$, where e_x is the unit vector in the streamwise direction).

In regard to species transport, mainly convective/diffusive transport was observed in the spanwise and streamwise directions. Figure 5a shows that steady flow species transport in large aspect ratio channels is not affected by the local velocity distribution. Hence, it can be assumed that streamwise velocity (u) in the species transport equation (2) can be approximated by the channel averaged streamwise velocity ($\bar{u}$). Under these simplifications, the steady species transport equation is reduced to:

$$\bar{u}\frac{\partial \Theta}{\partial x} = \frac{1}{Pe}\left[\frac{\partial^2 \Theta}{\partial x^2} + \frac{\partial^2 \Theta}{\partial y^2}\right], \tag{4}$$

where $\bar{u}$ is normalized with the reference velocity (U). Since the channel-averaged velocity is a constant over the entire domain, without a loss of generality, it can be stated that $U = \bar{u}$.

A further simplification can be made using an order of magnitude analysis. Namely, the streamwise diffusion was negligible compared to the spanwise diffusion (ie., $\partial^2\Theta/\partial x^2 << \partial^2\Theta/\partial y^2$).[50]   Hence, equation (4) can be reduced to the following form:

$$\bar{u}\frac{\partial\Theta}{\partial x} = \frac{1}{Pe}\left[\frac{\partial^2\Theta}{\partial y^2}\right] \tag{5}$$

An analytical solution of (5) was obtained for half of the channel using a separation of variables technique. The incoming fluid had concentration value of Θ_0, while at the channel center (y=h/2), $\Theta_c = \Theta_o/2$. This value was fixed along the entire channel ($0 \le x \le L$), due to the presence of a zero-concentration equal flow rate stream on the upper half of the domain. On the bottom wall (y=0), zero Neumann conditions ($\partial\Theta/\partial y = 0$) are assumed. Based on these boundary conditions, the analytical solution of (5) becomes:

$$\frac{\Theta - \Theta_c}{\Theta_0 - \Theta_c} = \sum_{n=0}^{\infty}\frac{2(-1)^n}{\left(n+\frac{1}{2}\right)\pi}\exp\left(-\left(n+\frac{1}{2}\right)^2\pi^2\frac{4x}{hPe}\right)\cos\left(\left(n+\frac{1}{2}\right)\pi\frac{2y}{h}\right) \tag{6}$$

Using equation (6), streamwise concentration variations were identified as a function of the diffusion distance x, the Pe number and the width of the channel (h), which together form a non-dimensional parameter:

$$\kappa = \frac{x}{hPe} = \frac{x\alpha}{h^2\overline{u}} \tag{7}$$

In Figure 6a, a typical concentration variation in the spanwise direction across half of the main channel (at κ=0.0052) is presented. This was obtained by three- and two-dimensional solutions of equations (1-3) using CFD-ACE+ and our spectral element algorithm,[50] as well as the analytical solution given by (6). Concentration variations in the spanwise direction obtained with an increased level of simplifications are similar to the three-dimensional solution. Detailed comparisons between the three- and two-dimensional simulations and the analytical model can be found in.[51]

Local values of κ were used to determine the concentration variation at any location in the channel. Since zero Neumann conditions on the walls are specified, the wall concentration value was also determined using the analytical (or numerical) solution. Figure 6b shows the variation of the side wall concentration (Θ/Θ_o) as a function of κ. This figure was obtained by a superposition of five different simulations at various Pe numbers, and also by evaluating the analytical solution at y=0. Due to the problem definition, the normalized right and left wall concentrations were related to each other in the following form:

$$\Theta/\Theta_o|_{\text{right-wall}} = 1-\Theta/\Theta_o|_{\text{left-wall}}$$

In addition, a unique concentration profile exists for any given κ. Figure 6b shows the normalized concentration distribution obtained at various κ values. The symbols and lines show the analytical results and the two-dimensional spectral element
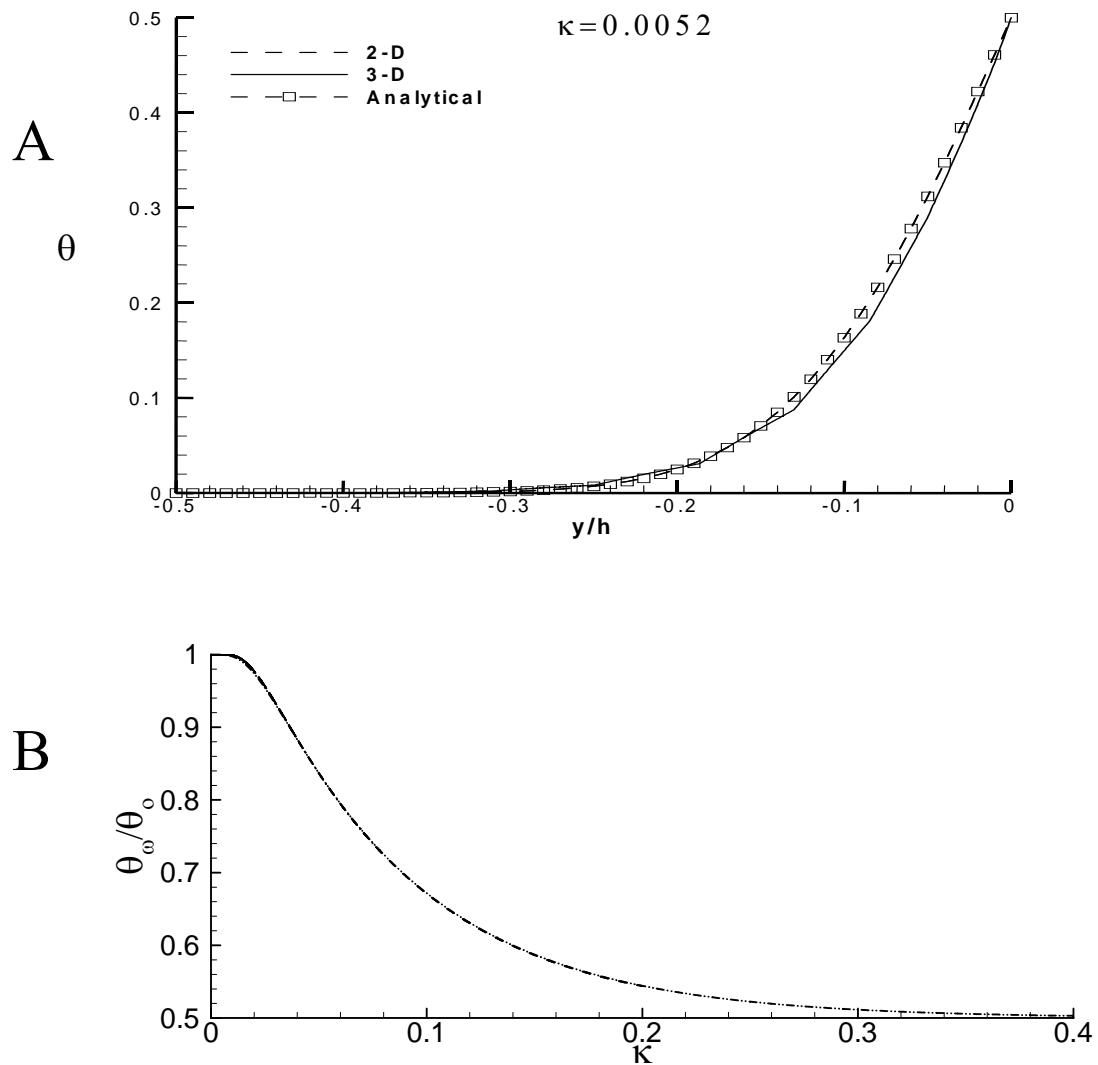
Figure 6. (a) Concentration variation across half of a channel at κ=0.0052. Comparison of prediction of three- and two-dimensional simulations with the simplified analytical model. (b) Top wall concentration variation as a function of κ. Five different simulations at various Pe numbers are plotted to obtain the curve.

solutions, respectively. Concentration profiles obtained in this section were used to evaluate the inlet conditions for numerical simulations of the μDD device.

Experimental Section

Glass Microchip Fabrication. Standard 50 mm x 75 mm soda-lime microscope slides were spin coated with Microposit S1813 photoresist (Shipley, Marlborough, MA) to a thickness of ~7 μm and baked in a convection oven at 90 °C for 1 hour. The photomask was produced by reducing a negative image printed from a 1200 dpi laser printer onto Kodak technical pan photographic film (which ultimately served as the contact photomask) using a Pentax K1000 camera fitted with an SMC Pentax-A 1:2 50 mm lens. Samples were exposed using a Quintel 6000 mask aligner and developed in a 1:1 solution of Microposit developer concentrate (Microchem) and DI water. Slides were etched and bonded using a process adapted from Lin and coworkers.[26] Photopatterned slides were gently wafted by hand in a BOE (buffer oxide etchant) solution (1:6 ratio of 48% HF:200 g NH_4F in 300 mL DI water) for 2.5 - 3 minutes and washed in a 1 M HCl solution for 20 min. The dimensions of the etched pattern are shown in Figure 7. Inlet holes 1 mm in diameter were drilled into the glass using a diamond coated drill bit (Wale Apparatus). A 25×37.5 mm planar soda-lime glass slide section was used as a cover for the channel system. Covers and etched chips were cleaned by boiling in 7X detergent and then placed in a warm 6:1:1 DI water:HCl:H_2O_2 solution for 5 minutes, a warm 5:1:1 H_2O:NH_4OH:H_2O_2 solution for 5 minutes, rinsed with copious DI water and dried with N_2. Devices were bonded by stacking the plates between weights in the following order: 0.5" thick solid brass substrate (which served as
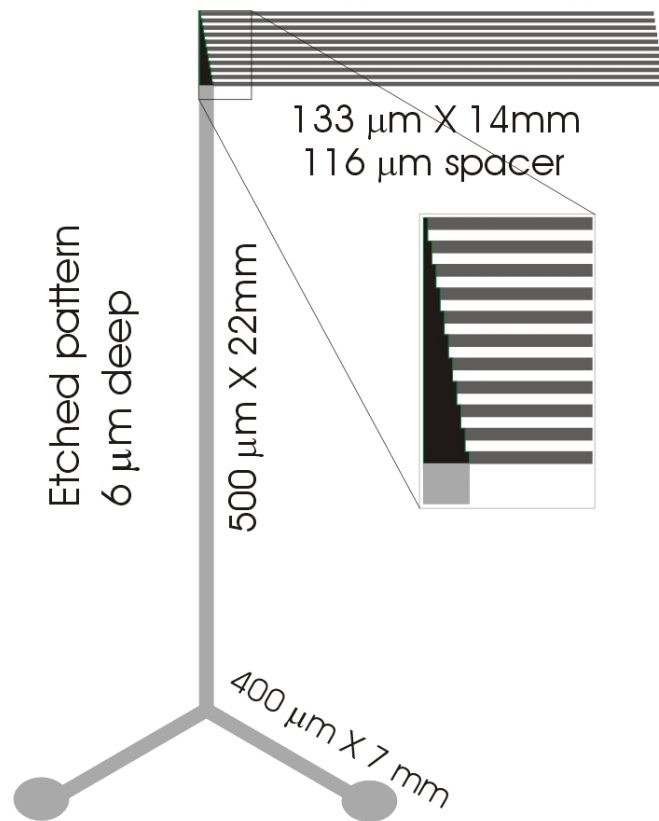
Figure 7. Microfluidic diffusion diluter dimensions. Microchannels are dark gray, splitting region in black, and main channel and inlets in gray.

a base), a polished alumina flat, the etched chip (channels up), a soda-lime cover, a second smaller polished alumina flat, and finally a 40 g brass weight. During thermal bonding, the weight would press on the alumina flat causing the two glass surfaces to fuse. After a first firing, the weight and the flat would be moved to an unbonded section and the firing schedule rerun. This process was repeated until all vital areas were bonded.[52] The firing sequence was as follows: from room temperature a 280 ºC/hr ramp was applied up to 400 ºC and held at that temperature for 4 hours. Next, a 280 ºC/hr ramp was applied up to 588 ºC and held for 6 hours. Finally, the kiln was shut off and allowed to cool back to ambient temperature.

Syringe Pump Modification. A syringe pump (PHD2000, Harvard Apparatus, Holliston, MA) was employed to pump liquid into the glass device. Since the pump's stepper motor turns 1.8° per step, pulsing in the flow was visible at very low speeds. To correct this, a 100.56:1 speed reducer gearbox (Berg, East Rockaway, NY) was retrofitted inline with the drivescrew of the pump. This caused the motor to turn 100.56 times for each turn of the drivescrew, significantly smoothing the motion of the pusher block (and thereby the flow) at low speeds. This also reduced the minimum and maximum speed of the pump by 2 orders of magnitude. The pusher block of the pump was modified in several respects. First, the bushings through which the block's guide rails align were replaced with linear bearings (PIC Design, Middlebury, CT). Aluminum blocks were attached on each side of the block behind the bearings to extend the overall length of the pusher block by 2.5." Additional linear bearings were fitted to the rear of the new aluminum blocks to give the pusher block assembly a total of 4 linear bearings.

Furthermore, the stock guide rails were replaced with precision-machined steel rails (PIC Design), which were exactly matched to the linear bearings. Finally, a custom adapter was machined to fit to the front of the pusher block, which had thumbscrew fittings that directly attached the syringe plunger to the block. These modifications eliminated slip-stick friction and pulsation under slow flow conditions. The modified pump was fitted with two 100 μL syringes (Hamilton, Reno, NV) and PTFE lines were attached with PEEK ¼-20:10-32 fingertight adapters (Upchurch, Oak Harbor, WA) and run to a homemade manifold for interfacing with the glass chips.

Fabrication of Chip Holder and Flow Rate Experiments. A Plexiglas manifold was machined with 2 inlet ports into which Teflon lines and PEEK fingertight fittings were inserted. This manifold was fastened to an aluminum chip clamp. A screw mounted over each outlet from the manifold clamped the chip into place with the inlet holes directly over the manifold outlet. The pressure from porous Teflon pads at the end of the clamp screw pressed the chip against Teflon o-rings and flattened them slightly to form a high-pressure seal. The Plexiglas/aluminum chip assembly was mounted onto the stage of an E800 microscope (Nikon). Using the modified syringe pump, the flow rate was varied and images were taken using a Micromax 1024 CCD camera (Princeton Instruments) atop the microscope. Data was collected using Metamorph software and normalized using Sigmaplot.

Results

    Dilution Experiments in Glass Microchips. To demonstrate the µDD concept, the modified syringe pump was used to inject an aqueous green fluorescent dye, Alexa 488, and an aqueous red fluorescent dye, Alexa 594, by positive pressure (100 nL/min) into the two inlet ports of the device. As the pump infused the dyes, diffusional mixing occurred over a ~22 mm path length before the liquid stream was separated into a series of 23 parallel microchannels. The array was imaged by epifluorescence microscopy (Figure 4b). As can be clearly seen, the concentration gradient present at the end of the main channel was continuously isolated and maintained in the microchannel array. The channel on the far left-hand-side contained mostly Alexa 488 while the channel on the far-right contained mostly Alexa 594. In between, the channels held a stepwise gradient of concentrations. This is shown quantitatively in Figure 4c by the line profile of fluorescence intensities.

    To investigate the effect of flow rates on the distribution of Alexa 594, the pump was run at several speeds varying from 50 nL/min to 500 nL/min. In this case an 11 channel device was employed to accommodate fluid dynamic calculations, which became increasingly time consuming as more channels were added. The line profiles for four flow rates are shown in Figure 8. At the highest rate, the concentration was only moderately distributed across the series of channels. From right to left, the concentration of the dye molecule increased from background noise to its maximum across only 7 channels. This was representative of how a high flow rate only allows for minimal diffusion. The difference between the channels with the highest and lowest dye
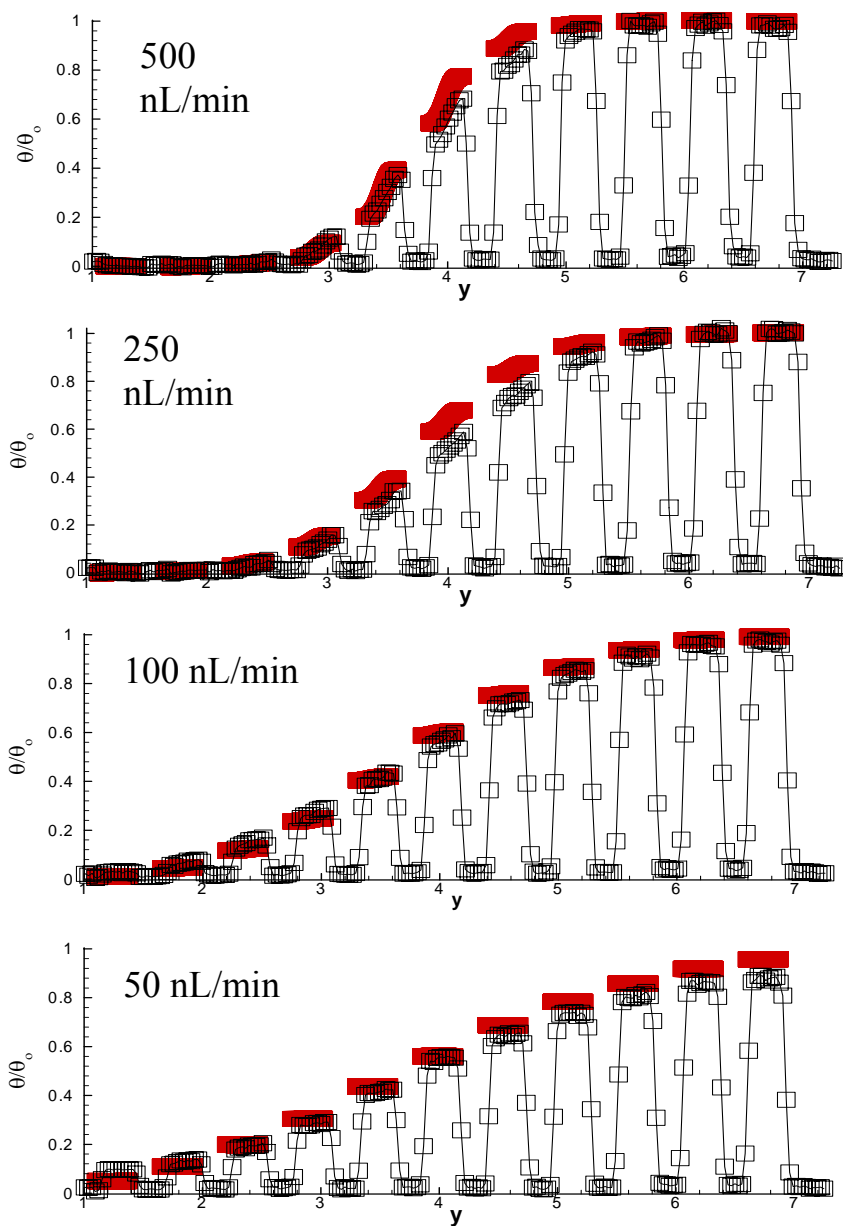
Figure 8. Spanwise concentration variation of the concentration profile after separation into the microchannels. The squares represent experimentally measured normalized intensity values, and the thick blocks represent computational values.

concentrations was at least 3 orders of magnitude and probably more. The ability to place an upper boundary on this value was ultimately limited by the dynamic range of our CCD camera. Slowing the flow rate to 250 nL/min spread the dye over 8 of the 11 channels and 100 nL/min covered 10 microchannels. Finally, at 50 nL/min, the Alexa 594 had migrated to cover all the channels. Fits to this data (shown as bars) using computational fluid dynamics, are described below.

Computational Modeling. The convective/diffusive transport problem was divided into two different parts: the main channel and the microchannels. The main channel section was modeled using the analysis presented in the theory section. On the other hand, the microchannel array was simulated using a two-dimensional spectral element algorithm, which is essentially a high-order finite element method.[50] Equations (1-3) were solved on a computational domain, geometrically similar to the actual μDD. Details of the computational domain and the independent grid studies can be found elsewhere.[51]

For comparisons of numerical and experimental results, the experimental data were normalized by using the maximum fluorescence intensity in the main channel obtained from the 500 nL/min case. The normalized fluorescence intensity distribution at the entry of the μDD (at x=21.4 mm) is shown in Figure 9. Comparisons of the experimental measurements with theoretical analysis required accurate predictions for the diffusion coefficient for the Alexa 594 dye. In order to determine the diffusion coefficient, the measured fluorescence intensity for the 500 nL/min case was matched with the theoretical model given by equation (6). The concentration distribution at
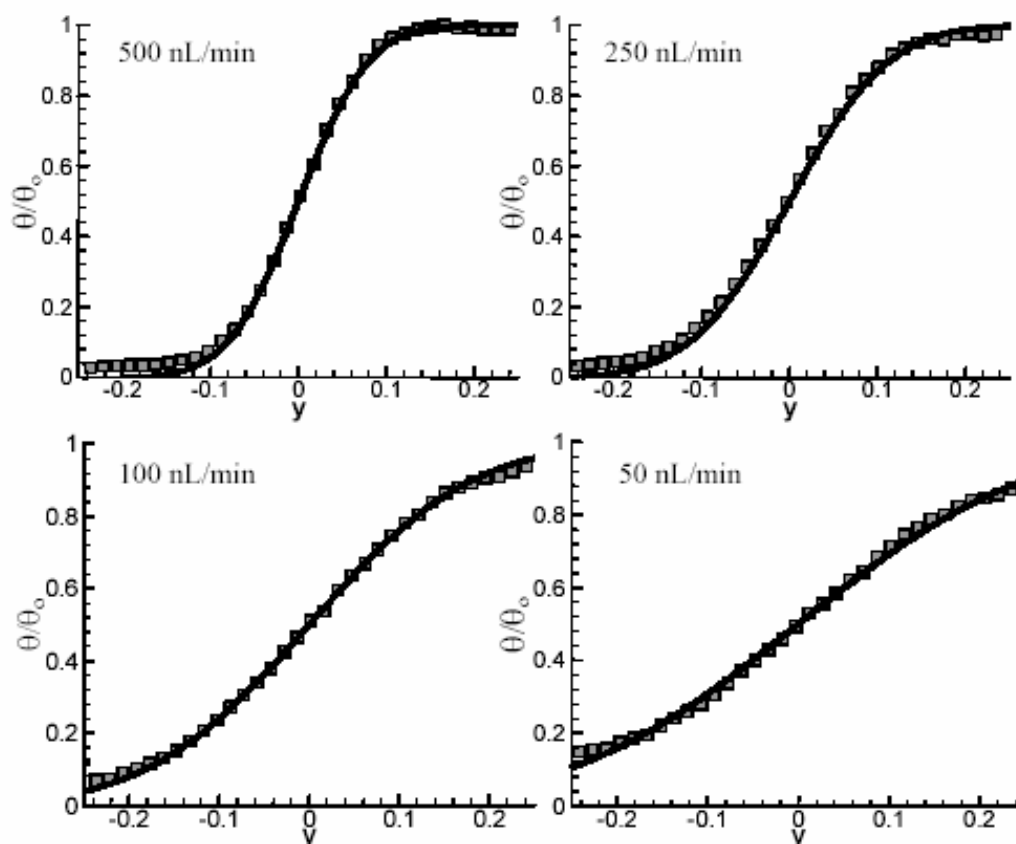
Figure 9. Main channel analysis. The gray squares represent fluorescence linescans across the width of the main channel and the lines are the predicted concentration profiles. (a) 500nL/min (b) 250 nL/min (c)100 nL/min (d) 50 nL/min.

κ=0.002 matched the normalized intensity measurements quite well. Using this one-point matching at κ=0.002, as well as the channel averaged velocity (2.543 mm/s) and the channel width (500 μm), the Pe was calculated to be 21,400 from equation (7). This value of Pe requires a molecular diffusion coefficient of $\alpha = 6.5 \times 10^{-11} \, m^2/s$. In Table 1, the κ values, Re and Pe numbers obtained for all the flow rates (500 to 50 nL/min) are shown. Agreement between the experimental measurements and the theoretical results was observed over a wide range of flow rates. This validates the consistency between the numerical results and the experimental measurements.

The theoretically obtained concentration variations were utilized as the inlet (boundary) conditions for numerical simulations of the μDD as well as for the calculated concentration profiles in the output channels (bars in Fig. 8). For all cases, experimentally measured fluorescence intensity values were normalized against the fluorescence intensity of the 500 nL/min flow rate. The final concentration profile in the 500 nL/min case did not diffuse much after entering the microchannels. This was expected, since the Pe number was quite high and the process was almost entirely convection dominated. At 500 nL/min, the first 3 microchannels experience concentration values close to Θ=0, while the last 4 microchannels have values near Θ=1. The results for the 250, 100 and 50 nL/min cases are also shown in Figure 8. As expected, the diffused zone in the middle of the micro channels grows with decreased flow rate. Overall, the computational results closely follow the experimental measurements. Hence, it is possible to generate a desired concentration variation in the

Table 1.

Flow rate(nL/min)	Kappa	u_{avg}(m/sec)	Re = u_{avg} h/ν	Sc = ν/D	Pe=Re*Sc
500	0.002	$2.78*10^{-3}$	1.389	15406.76	21400
250	0.004	$1.39*10^{-3}$	0.6945	15406.76	10700
100	0.01	$0.556*10^{-3}$	0.2778	15406.76	4280
50	0.02	$0.278*10^{-3}$	0.1389	15406.76	2140

μDD, and theoretical and numerical models can be used to accurately predict the underlying physics and μDD performance.

Discussion

In the experiments presented above, a right angle geometry was employed to separate the main channel into distinct microchannels. Though other geometries were tested, this particular layout proved superior because the streamwise velocity remained constant throughout the main channel and microchannels. Furthermore, the design enabled efficient packing of the device onto a relatively small rectangular chip. As mentioned above, this design has consequences for the distribution of concentrations in the microchannels. Namely, the inflection point of the concentration distribution in the microchannels does not center around the middle microchannel, even though the concentration distribution is symmetric in the main channel. In fact, the inflection point is closer to the first microchannel in all cases. This asymmetry arises from the fact that the left wall of the main channel was 3 mm (black region in Fig. 4) longer that the right side. However, this makes no practical difference in terms of assay development, since the analyte concentrations can be calculated or quantified experimentally in each channel by fluorescence measurements.

Myriad chemical and biochemical processes are concentration dependent. This fact has traditionally forced researches to undertake the laborious task of preparing serial dilutions for step-by-step analysis of concentration dependent phenomena. Recently, several research groups have constructed various on-chip dilution devices to circumvent this problem.[40,42,44] The first approach by Ramsey and coworkers used electrokinetically

driven methods. This device is limited to conducting solutions and may lead to sample damage by Joule heating in certain cases. Whitesides and coworkers designed a pressure-driven device that employed a branching mechanism. This required an entire mixing row for every new channel added to the array. Although such devices are capable of producing linear concentration gradients, they require long mixing lengths, have comparatively large dead volumes, and consume relatively large amounts of precious analyte due to fast flow rates.

The development of μDD was motivated by the need to obtain the maximum amount of data from the minimum amount of sample. Indeed, this technique can be expanded to probe a variety chemical systems.[34,53] For example, the array-based field of proteomics could benefit from μDD because of its capability to collecting massive amounts of data from a few microliters of newly isolated protein. Specifically, glass microchips could be employed to investigate the various concentration dependent behaviors of protein/ligand interactions and, thus, rapidly obtain kinetic and thermodynamic parameters. This could be done by creating a concentration gradient of protein over a chemically modified ligand-containing surface to study binding affinity.

Conclusion

We have designed and characterized a microfluidic diffusion diluter for the combinatorial study of concentration dependent phenomena. In high aspect ratio systems, it is reasonable to simplify three-dimensional numerical simulations to two dimensions, since diffusion dominates spanwise transport and convection dominates streamwise transport of analyte. We have developed a non-dimensional parameter

κ, which describes this process and allows the efficient prediction of concentration values in the µDD.

CHAPTER IV

MICROFLUIDIC DIFFUSION DILUTER: BULGING OF PDMS MICROCHANNELS

UNDER PRESSURE-DRIVEN FLOW*

Introduction

Polydimethylsiloxane based microfluidics has proven to be a fast, cheap and widely accessible technology for rapid prototyping in microanalytical systems.[13] Replica molding with PDMS can be employed for making valves, pumps, electrophoretic separation systems, gradient generation as well as for many other processes.[28,31,34,41-43,52,54-56] Further PDMS advantages include optical transparency and easily modified surface chemistry.[32-34,56-58] However, aspect ratio becomes a major design constraint in these systems, since very wide and shallow microchannels can easily collapse during the bonding process.[59] Though electroosmotic and vacuum driven flow[60] through such PDMS devices can be carried out with relatively little concern for microchannel geometry changes, positive pressure-driven flow presents a unique set of challenges. Specifically, there is a serious consideration for pressure-driven flow through such microchannels, which has been largely overlooked. Namely, the pressure itself can induce a ballooning effect that greatly increases the cross-sectional area of the microchannel during flow. This phenomenon and its effect on creating dilution gradients is the central concern of this Chapter.

Chapter III demonstrated a pressure-driven device for isolation of concentration gradients in a rigid, all glass microchip. The technique, called microfluidic diffusion

dilution (μDD), works by combining two flowing streams at a Y-junction into a main channel, which is subsequently divided into a parallel array of microchannels. Each channel contains a successively higher concentration of a given analyte, and the shape and distribution of the gradient formed is a function of the flow rate. Numerical simulations were successfully used to predict how the concentrations would be distributed in the microchannels. It would be convenient to extend this methodology to PDMS/glass hybrid systems, but due to the elastic nature of PDMS, the channel geometry changes as a function of flow rate. This, in turn, affects the convective/diffusive transport of analytes in the μDD.

Figure 10a shows a cartoon representing the main channel under conditions of pressure-driven flow. The channel would be a rectangular duct under no-flow conditions (blue rectangle in Fig. 10a); however, the cross-section takes on a hemi- cylindrical shape at high flow rates. This cross-section "deflates" as the fluid moves downstream. Not only does the channel geometry change as a function of position, but also the channel-averaged velocity of the fluid is affected. In Figure 10a, the last segment, shown in green, represents the end of the main channel just before the microchannel entrance. When fluorescence intensities are measured here in an actual device as a function of flow rate, dramatic geometric changes can be seen. Epifluorescent data of Alexa 594 dye in buffer solution inside the main channel and channel array clearly show that the channel cross-sectional area expanded with increasing of flow rate (Figure 10b). The bulging effect on the microchannels was not as pronounced as in the main channel.
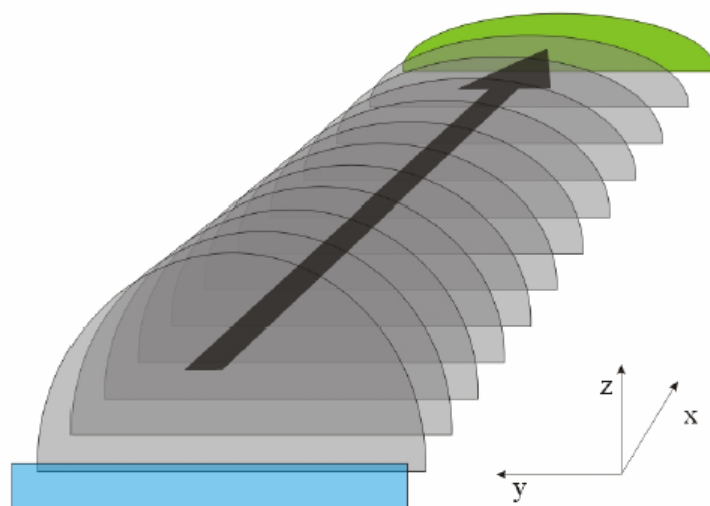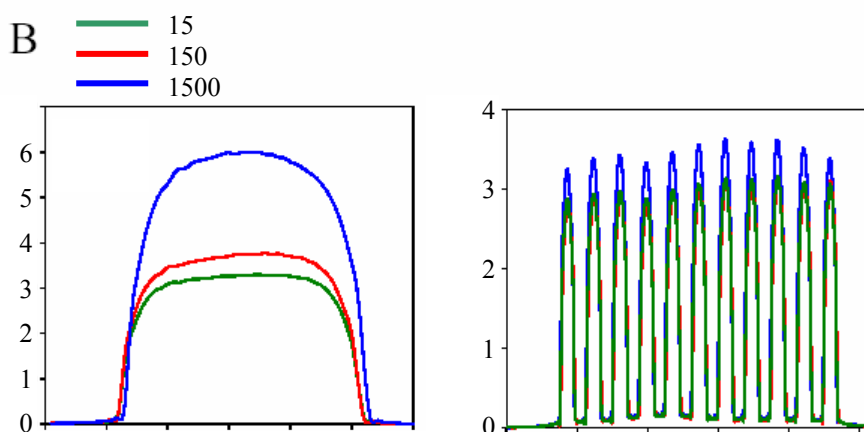
Figure 10. (A) Schematic representation of a bulging microchannel under pressure-driven flow (not to scale). The original geometry under no flow conditions (blue) expands greatly at high flow rates (gray). (B) Background subtracted fluorescence intensities taken across the width of the main channel just before the inlet to the microchannels (left) and across the microchannels (right) at various flow rates. Flow units shown in the legend are in nL/min.

because the microchannels have a higher combined cross-sectional area and lower aspect (width to height) ratios

Experimental

Device Fabrication. Standard 50 mm x 75 mm soda-lime microscope slides were spin coated with Microposit S1813 photoresist (Shipley, Marlborough, MA) to a thickness of 6 μm and baked in a convection oven at 90 °C for 1 hour. The photomask was produced by reducing a negative image printed from a 1200 dpi laser printer onto Kodak technical pan photographic film (which ultimately served as the contact photomask) using a Pentax K1000 camera fitted with an SMC Pentax-A 1:2 50 mm lens. Samples were exposed using a Quintel 6000 mask aligner and developed in a 1:1 solution of Microposit developer concentrate (Microchem) and DI water. Glass barriers were glued around the photopattern and degassed PDMS was poured and cured in a convection oven at 70 °C for at least 3 hours. Molds were peeled away and a piece of PDMS was sliced off to open the microchannel outlets. Using a hollow flat-tipped syringe needle, holes were reamed to form the two inlets to the device. The PDMS mold and a clean 25 mm x 50 mm microscope cover slide were simultaneously placed in a plasma cleaner and oxidized for 20 sec. The two pieces were brought immediately into contact to form an irreversible bond. Water was injected as quickly as possible into an inlet port of the nascent device to hydrate the channel. This insured that the main channel did not collapse and bond with the surface during subsequent use.

Epifluorescence Microscopy Flow Rate Experiments. Fluorescence data was acquired with a Nikon E800 microscope using a Pentamax CCD camera (Princeton

Instruments). The PDMS/glass device was attached to the microscope stage and two Teflon lines were inserted into the inlet ports. A modified syringe pump (Harvard Apparatus, Holliston, MA) fitted with 2 Hamilton 100 μL syringes, where one syringe was filled with buffer solution and the other with buffer solution plus Alexa 594 dye, pumped the fluid. Data were acquired using Metamorph (Metamorph 5.0r1, Universal Imaging Corp.) software and normalized in Sigmaplot.

Results and Discussion

Since the bulging of the PDMS channels changed the pathlength through the dye solution, it was possible to directly determine the channel height as a function of flow rate with a constant concentration of solution. This was achieved by infusing identical concentrations of fluorophore into both inlets to the main channel. Figure 10b shows the fluorescence profile taken across the main and microchannels at various flow rates. The fluorescence intensity observed was approximately twice as high in the main channel at 1500 nL/min as at 15nL/min despite the fact that the dye concentration remained the same everywhere in the fluid. This was a direct indication of the path length increase and, hence, channel bulging. Note that the effect of flow rate on bulging is much stronger for the main channel than the microchannels. This was due to the fact that the microchannels taken in aggregate have a greater cross-sectional area than the main channel and, therefore, the pressure was lower. Due to the constant drop in pressure as the fluid moves downstream, the force "inflating" the microchannels is also lower than that of the main channel. Furthermore, the aspect ratio of the microchannels is significantly lower, thereby enhancing the mechanical rigidity of microchannels.

Conclusion

  We have built a microfluidic diffusion diluter using PDMS and performed experiments for various flow rates over two orders of magnitude. The PDMS device bulged when the flow rate was high and relaxed when it was low.

CHAPTER V

LIGHT ACTIVATED PATTERNING OF DYE-LABELED MOLECULES ON

SURFACES*

Introduction

Since the late 1980's, a number of photoimmobilization strategies have been developed for producing patterns of proteins on a variety of surfaces.[61,62] Several approaches work by photochemically modifying surfaces to either promote or deter non-specific protein or cell adsorption.[61,63-69] Other methods employ a variety of photoactive moieties, which can link specific ligands or proteins of interest to the surface. For example, arylazides and aryldiazirine moieties have been used to capture proteins in patterns via light activation to highly reactive nitrenes[70-72] and carbenes.[73-78] Benzophenone groups have been employed to create reactive benzhydrol radicals.[79-82] Various forms of deprotection chemistry using nitrobenzene as a caging moiety have also been used to pattern active surfaces.[20,83-86] Two particularly popular strategies employ caged biotin[87,88] and photobiotin,[89-91] which exploit the ubiquitous biotin-avidin/streptavidin interaction.

Although these diverse methods have proven very useful, they nevertheless possess certain drawbacks. For example, all of them require the use of UV radiation (typically 350 nm) to perform the immobilization. Also, many of the small molecule cross-linkers are not readily available in highly water-soluble form, and are often spun on and dried before irradiation. It would be highly desirable to develop methods by

---

which ligands and/or proteins of interest could be patterned in aqueous environments with longer and less damaging wavelengths. In fact, if linking chemistries were available at a variety of longer wavelengths, it should be possible to pattern several different species onto the substrate from a single solution simply by exposing different wavelengths of light to different portions of the surface. Below we lay out a general strategy for light induced surface patterning by employing commercially available dye molecules that react over a broad range of wavelengths. This method also enjoys the benefit of being compatible with aqueous solution chemistries.

Fluorescent dyes represent an incredible diversity of compounds excitable over a wide range of wavelengths. Prolonged exposure of these molecules to light generally leads to photobleaching and loss of fluorescence.[92] While this effect is usually an undesirable byproduct in most applications, photobleaching could also be exploited to create photogenerated radicals[93] for attaching organic linker molecules to substrates. Indeed, it should be possible to covalently pattern dye-conjugated ligands to a substrate under aqueous conditions by following the simple strategy outlined in Figure 11.

Experimental

Microscope Photopatterning. Small wells were created by reaming 9 mm holes through PDMS slabs and subsequently pressing the nascent mold against clean glass coverslips. All protein solutions and fluorophore solutions were prepared using the same pH 7.4, 150 mM ionic strength PBS buffer. BSA (bovine serum albumin, Sigma) solutions were prepared at 0.5 mg/ml and biotin-4-fluorescein prepared at 0.05mg/ml. Alexa 594 labeled IgG and Alexa 488 labeled streptavidin were purchased from
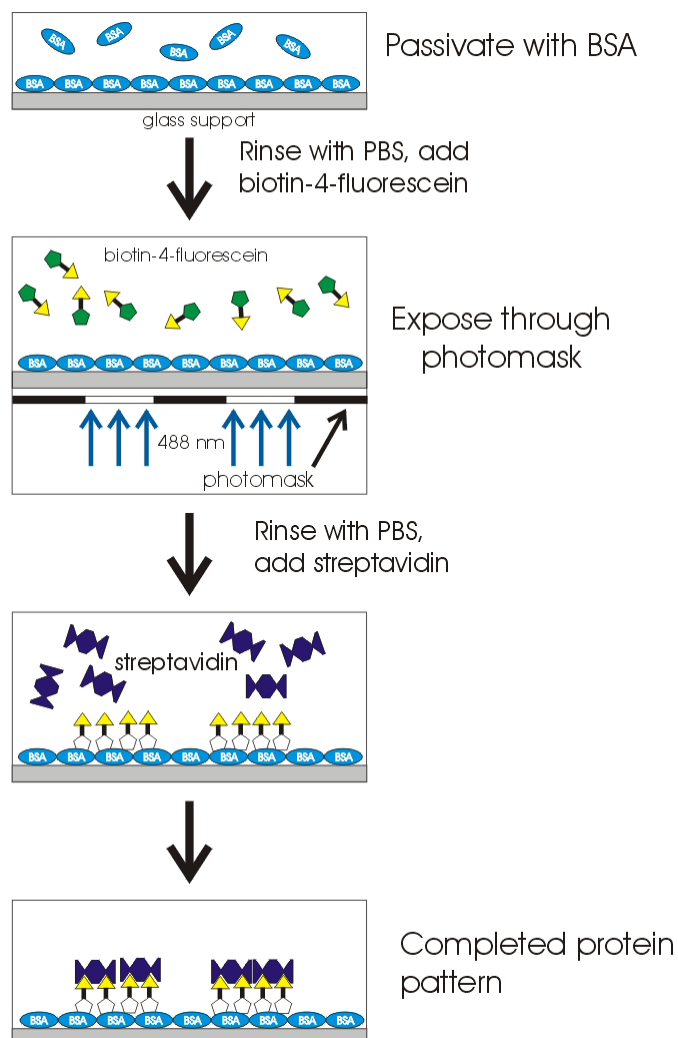
Figure 11. Photobleach micropatterning. First, a passivation layer of bovine serum albumin (BSA) is deposited onto a glass substrate from a buffer solution. The excess BSA is washed out followed by the introduction of an organic fluorophore containing a covalently attached ligand. Fluorophores are excited on resonance causing photobleaching and attachment to the passivated substrate via a mechanism involving singlet oxygen.[94] Although the fluorophore is destroyed in this process, the ligand molecule is bound to the interface and available for attachment by a protein.

Molecular Probes (Eugene OR) and diluted to 0.5 mg/ml in PBS. For patterning, the PDMS/glass wells were filled with BSA solution and incubated at room temperature for at least 10 minutes. The well was then rinsed with PBS buffer, followed by the introduction of the biotin-4-fluorescein /IgG solution. The stamp with the solution was inverted and placed on the stage of a Nikon E800 upright microscope. A photomask was placed against the glass of the inverted mold and secured with a drop of objective immersion oil. Using the 4x objective, 560 nm light filtered from an Hg arc lamp (20 mW) was used to expose the IgG for 2 hours. The mask was rotated about the center of the cross 45 degrees and the filter sets on the microscope adjusted to illuminate with 488 nm light to bleach the biotin-4-fluorescein. After exposure, the solution was rinsed out with PBS buffer. Next, Alexa 488 labeled streptavidin solution was introduced and incubated for 2 minutes, followed by a final PBS rinse. Fluorescence images were taken with a CCD camera under the E800 microscope. False color micrograph images were produced using Photoshop (Adobe).

Laser Photopatterning and Determination of Resolution. The fidelity of this patterning process is likely limited to two basic experimental conditions. First, the degree to which light at the desired wavelength can be collimated and subsequently passed through a high resolution photomask, and second, the lifetime subsequent mean diffusion distance of an activated fluorophore combine to counter the ability to produce sharp edge features. To explore this limit, we patterned BF on a BSA coated microscope cover slip by passing the 488 nm line of a Ar ion laser (300 mW) for 1 second through a high resolution chrome on quartz test mask (Edmund Optics). After washing with PBS,

Alexa 488 streptavidin was allowed to bind to the immobilized biotin and fluorescence images were taken. The resulting pattern is shown in Figure 12. This process produced resolved features down to about 7 microns, and could probably be smaller with a more collimated light source. Our laser is slightly divergent, and diffraction patterns are clearly visible in the features below 7 microns. Therefore, this process is more likely to be limited by diffraction issues rather than lifetime and diffusion of activated molecules.

Results and Discussion

As a demonstration of this principle, surface patterning was performed by bleaching two fluorophore-labeled species sequentially onto a BSA coated substrate from a single phosphate buffer solution (Figure 13). This process is quite general; therefore, it is not only possible to link small molecule ligands to the surface via photobleaching, but also to directly attach whole fluorescently labeled proteins. We demonstrated this process by using a PBS buffer solution containing 0.025 mg/ml of biotin-4-fluorescein and 0.25 mg/ml Alexa 594 labeled anti-dinitrophenyl IgG. Fluorescein can be photobleached with blue light, while the Alexa 594 can facilelybleach in the yellow/green region. Alexa 594 labeled IgG was patterned first by passing 560 nm light through a cross shaped photomask for 2 hours. Since each IgG contained 3-4 fluorescent labels, the protein pattern could clearly be visualized on the surface by its characteristic red fluorescence, since not all fluorophores were consumed during the attachment process. The photomask was then rotated 45 degrees and the biotin-4-fluorescein was patterned for 30 minutes using 485 nm light. Control experiments were performed by washing out the bulk solution showed no evidence for
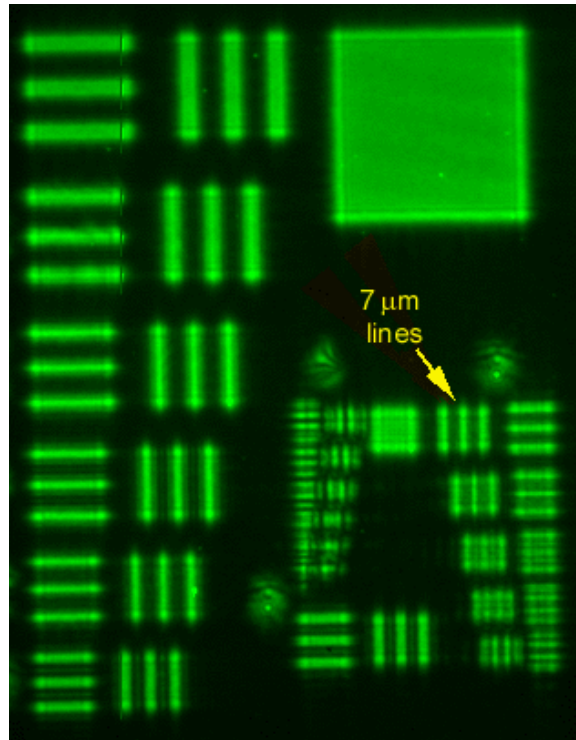
Figure 12. Image of Alexa 488 labeled streptavidin bound to patterned biotin-4-fluorescein produced with high resolution test mask. The marked lines are 7 microns in width.
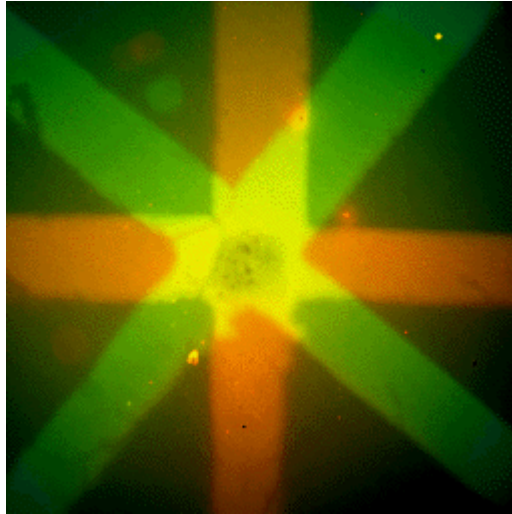
Figure 13. Sequential photopatterning of two different fluorophore linked species from the same solution. The red cross corresponds with the Alexa 594 labeled IgG and the green cross with Alexa 488 labeled streptavidin. Each patterned line is 250 microns wide, although line widths of 7 μm could be easily resolved with this technique. The dark region in the center of the intersecting lines is due to a reference dot (through which light could not pass during surface patterning) used to align the mask.

green fluorescence from the bleached species after surface patterning of the fluorescein dye. At this point, the aqueous solution was rinsed out and a solution containing Alexa 488 labeled streptavidin was introduced for 2 minutes. The sample was then rinsed with pure buffer and the surface imaged. As can be clearly seen, the streptavidin was patterned only where the 485 nm light was shined onto the surface, while the IgG was patterned where 560 nm light was irradiated.

In order to qualitatively examine the binding of streptavidin to biotin-4-fluorescein (BF) linked on the BSA coated surface, measurements of streptavidin binding were made as a function of time of BF photopatterning. Figure 14 shows a plot of fluorescence intensity from Alexa 594 labeled streptavidin bound to the biotinylated surface as a function of exposure time. As can be seen from the data, the amount of streptavidin that could be adsorbed increased almost linearly when the BF exposure time was low; however, above ~2000 seconds, the amount of streptavidin adsorption began to show saturation behavior. Since the size of the protein is far larger than the ligand, it is assumed that protein crowding limited the extent of adsorption.

To explore the mechanism of attachment of the fluorophore to the BSA coated surface, experiments were performed with varying concentrations of dissolved oxygen in the buffer solution. The effect of dissolved oxygen content on the efficiency of photopatterning BF was examined both in the absence of dissolved oxygen and in the presence of saturated solution. To prepare oxygen depleted solutions, natively dissolved gasses were removed from the BSA and BF solutions by vacuum, followed by a nitrogen purge. The BF containing solution was furthermore patterned over the surface in the
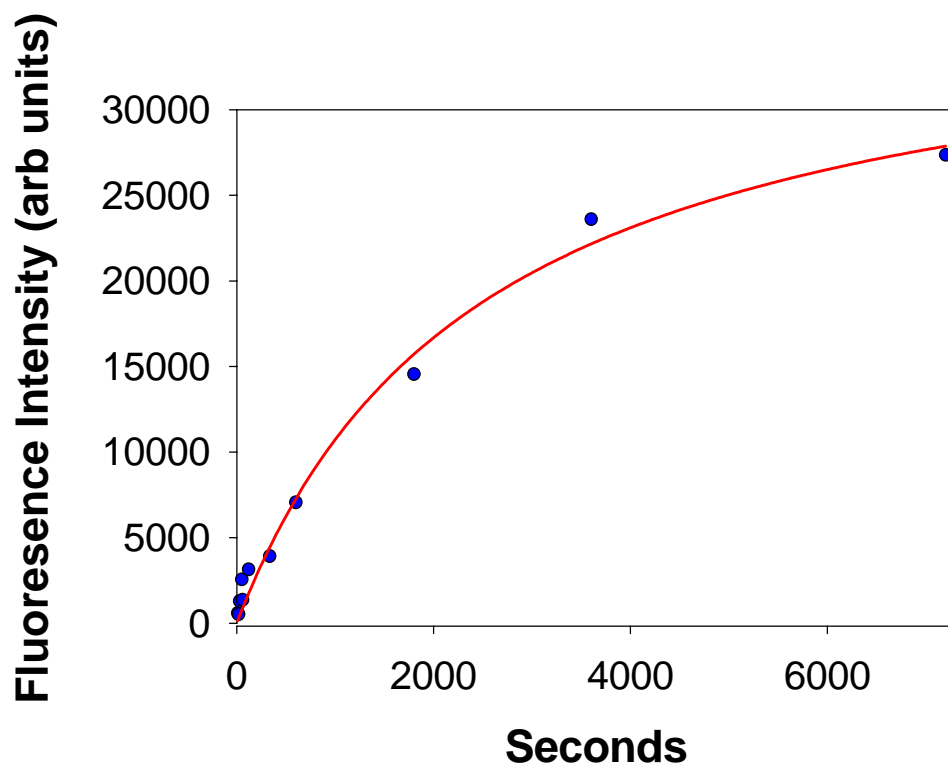
Figure 14. Plot of fluorescence from Alexa 594 labeled streptavidin bound to surfaces patterned with BF vs. time of exposure to 488 nm light. The red line is a least squares fit to the data**.**

presence of glucose oxidase and glucose to scavenge any additional oxygen that might be subsequently dissolved. On the other hand, a saturated oxygen solution was prepared by bubbling pure oxygen through the buffers for 15 minutes before use. Both the deoxygenated and saturated solutions were exposed to light for 90 seconds followed by rinsing and the introduction of streptavidin to the photopatterned surfaces. It was found that protein attachment was increased by a factor of seven in the presence of the saturated solution compared with the deoxygenated case. The left image in Figure 15 corresponds to the deoxygenated experiment while the right image represents the oxygen-saturated conditions.

The results indicated that solutions saturated with oxygen led to much more rapid photopatterning than buffer solutions that were oxygen depleted. This result is consistent with the idea that photobleaching of fluorescein (or Alexa dye) occurs through the formation of a triplet state, the binding of triplet oxygen, and the subsequent formation of singlet oxygen.[93] The highly reactive singlet oxygen probably attacks the fluorophore to generate a free radical species that can facilely bind with the BSA coated surface. This mechanism is also consistent with the observation that fluorophore attachment to bare glass was much slower than to a protein layer as was found by additional control experiments. This is almost certainly because glass contains relatively few electron rich sites for attack by free radicals.
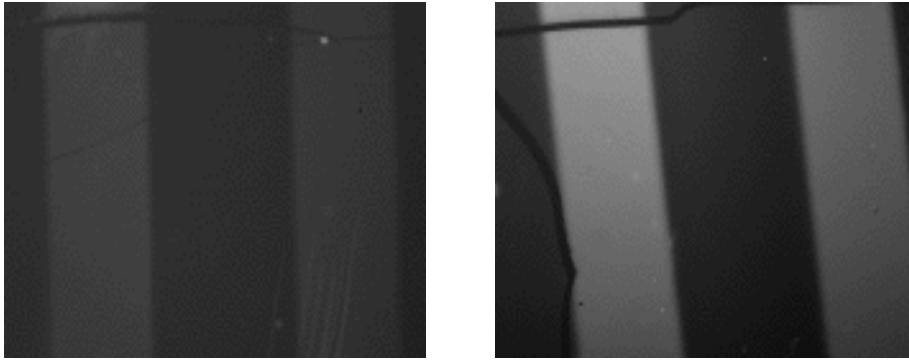
Figure 15. Dissolved oxygen comparison. The left image was photopatterned using solutions with low oxygen content while the right image was made using oxygen saturated solutions. All other conditions were identical. The thin dark lines in each image were scratches made intentionally for the determination of the background signal.

Conclusion

The technique described above has many potential applications. For example, biomolecules could be patterned inside microfluidic devices in an online fashion without the need to expose the materials to anything other than aqueous solution conditions. Furthermore, the technique could be expanded to the immobilization of DNA, peptide, or other material arrays. Finally, although the proteins patterned here were deposited sequentially from solution, it should be possible to deposit materials in parallel from a single solution provided light sources at multiple frequencies can be trained onto the surface simultaneously, as in Figure 16.

Figure 16. Simultaneous multipattern process. Two well-focused lasers of the appropriate wavelength could be used to pattern multiple fluorophore-labeled species from solution simultaneously, with high spatial resolution.

CHAPTER VI

PATTERNING ENZYMES INSIDE MICROFLUIDIC CHANNELS VIA

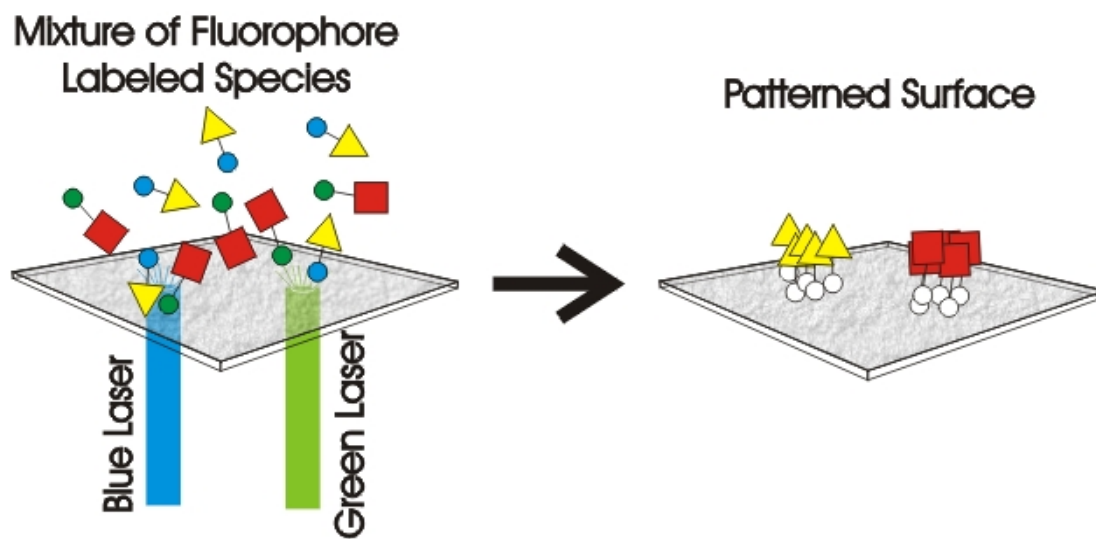PHOTOATTACHMENT CHEMISTRY*

Introduction

The use of microfluidic strategies for investigating the catalytic properties of immobilized enzymes has gathered significant attention in recent years.[3,34,56,95-100] Indeed, these techniques should enable the rapid testing of a library of biocatalysts as well as allow for the screening of an array of small molecule inhibitors against substrate binding in systems that require only minimum concentrations of analyte. Such impetus has led to the development of various lab-on-a-chip platforms for heterogeneous assays. For example, Kim et al. immobilized trypsin in sol-gel filled PDMS microchannels for monitoring fluorogenic substrate cleavage.[96] Similarly, Peterson et al. used *in situ* polymerization to form porous polymer monoliths into which trypsin was covalently attached.[97] Eteshola et al. demonstrated the feasibility of ELISA assays inside microfluidic devices,[56] while Crooks and coworkers provided several examples of heterogeneous enzyme catalysis employing hydrogels[95] and weir-dammed enzyme beads.[98,99] Endogluconase activity has been regulated using a photo-responsive polymer by Shimoboji et al.[100] In our own laboratory, we have immobilized enzymes on supported lipid bilayers to create one-shot Lineweaver Burke plots as well as for demonstrating the first example of a two-step enzyme microreactor.[34] Additionally, we have exploited temperature gradient microfluidics to make one-shot Arrhenius plots and

abstracted the corresponding activation energies for enzyme turnover.[53] While the above strategies are quite promising, a large issue remains unsolved. Namely, it can be time consuming and tedious to place enzymes at the appropriate locations on-chip. Since there is usually only limited control over positioning, it would be advantageous to find a route to enzyme immobilization which would rapidly pattern proteins at any desired location in a microfluidic network. Ideally, this could even be done from an aqueous solution after the device has been fully fabricated and enclosed. One potential route for accomplishing these tasks is the employment of a photoattachment strategy, whereby enzymes or linkers would bind to a channel surface from solution only at locations that are being exposed to light of a particular frequency. This would allow complex protein patterning networks to be created *in situ* inside a microfluidic device in a manner such that the enzyme would not have to be exposed to air, organic solvent, or other denaturing conditions. The challenge, of course, is that this method would necessarily require the photolinker chemistry to work in water-based solutions under mild conditions.

As a step toward this goal, we recently developed a simple, but widely applicable method for the attachment of photoactive molecules to protein-coated interfaces from aqueous solution near neutral pH and room temperature.[101] The process works by photobleaching fluorophore-linked species to generate short-lived, highly reactive free radicals capable of attacking electron-rich surfaces. For example, bovine serum albumin (BSA) coated glass coverslips could be patterned with a variety of proteins from phosphate buffered saline (PBS) with micron-level precision. Herein, we expand on this immobilization method to create well-defined patches of streptavidin-linked enzymes
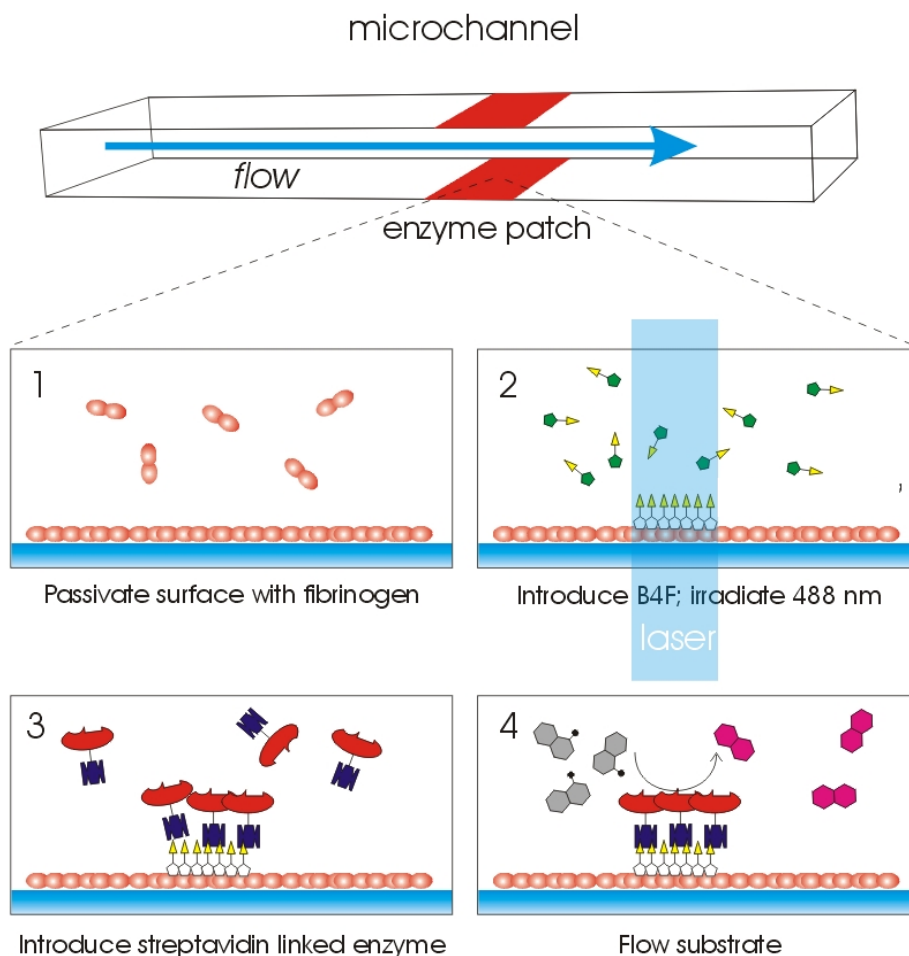
Figure 17. Schematic diagram of the photoimmobilization process. (Top) Enzyme patches are formed on the top and bottom of a microchannel using the following procedure: (1) Passivation of the surface with a fibrinogen monolayer is followed by (2) biotin 4-fluorescein surface attachment. This is accomplished by photobleaching with a 488 nm laser line. (3) Next, the binding of streptavidin-linked enzymes that can be exploited to immobilize catalysts and (4) monitor reaction processes on-chip.

inside microfluidic channels (Figure 17). For this purpose, bovine fibrinogen has replaced BSA as the surface coating layer due to its superior ability to present a large number of binding sites while preventing non-specific adsorption of the three enzymes investigated herein: glucose oxidase (GO), horseradish peroxidase (HRP) and alkaline phosphatase (AP). The addition of fibrinogen to the enzyme patterning solution also aided in the prevention of non-specific adsorption by out competing enzyme-linked-streptavidin for defect sites.[3,102]

Experimental

Microfluidic Device Fabrication. PDMS/glass microfluidic devices were prepared as previously described. [32] Briefly, 50 mm x 75 mm soda-lime microscope slides were spin coated with Microposit S1813 photoresist (Shipley, Marlborough, MA) to a thickness of 10 μm and baked in a convection oven at 90 °C for 1 hour. Photomasks were prepared as reduced negatives on photographic film with simple geometries consisting of 3 independent microchannels 32 mm long x 290 μm wide. A second pattern consisting of a 12 channel microarray with 130 μm widths was also made. Samples were exposed using a Quintel 6000 mask aligner and developed in a 1:1 solution of Microposit developer concentrate (Microchem) and DI water. Glass barriers were glued around the photopattern and degassed PDMS was poured and cured in a convection oven at 70 °C for at least 3 hours. Molds were peeled away and inlets were reamed at the channel termini using a hollow flat-tipped syringe needle. Next, the PDMS mold and a clean 25 mm x 50 mm microscope cover slide were placed in a plasma cleaner and oxidized for 20 sec. The two pieces were brought immediately into

contact to form an irreversible bond. The passivating protein solution was injected into the microchannels as quickly as possible to insure the surface of the PDMS remained hydrophilic.

Streptavidin Immobilization Assay. Fibrinogen, lysozyme, BSA, and IgGs (all from Sigma) were tested individually for their ability to form a passivating thin film coating on glass slides. In addition, they were probed for their number densities of specific binding sites for photoactivated fluorophores. Each protein was dissolved at various concentrations in pH 7.2, 150 mM PBS. The protein solutions were injected into individual microchannels of a 12 channel PDMS/glass array and allowed to incubate for 30 min. After incubation, fresh PBS was flushed through the channels to remove unadsorbed protein. Next, a solution of biotin-4-fluorescein (B4F, Molecular Probes), 0.05 mg/mL in PBS, was injected into all the channels. In order to surface pattern the B4F, the 488 nm line from an Ar^+/Kr^+ laser beam (Spectra Physics) was passed through a reducing telescope to produce beam diameters of ~300 μm (full-width half-max). The PDMS microfluidic device was scanned through the laser beam by mounting it on a syringe pump pusher block moving at a constant speed. This ensured that each channel was uniformly exposed to the same amount of light across the entire width. Typically, laser power of 150 mW and a scan rate of 1 mm/sec were sufficient to maximize the amount of biotin-4-fluorescein that could be photoattached. The photoattached patches were roughly 500-800 μm wide. PBS was used to rinse out excess biotin-4-fluorescein. At this point, about 200 μL of a 0.1 mg/ml Alexa 594 labeled streptavidin solution in PBS (which also contained 2.7 mg/ml unlabeled fibrinogen) was rinsed through the

channel. The fibrinogen was added to compete against streptavidin for any remaining non-specific adsorption sites on the surface. The solution was rinsed out of each microchannel after less than 1 minute. The resulting pattern of immobilized streptavidin could be imaged under a Nikon E800 epifluorescence microscope with a CCD camera (Princeton Instruments) using MetaMorph software.

Immobilized Single Enzyme Assay. Using the laser scanning procedure described above, B4F was patterned in consecutive patches inside PDMS/glass microfluidic devices that were previously incubated with 2 mg/ml bovine fibrinogen for 30 minutes. To make more than one patch along a single channel, a motion stage attachment was added to the syringe pump pusher to allow for movement normal to the direction of travel of the pusher block. This technique was employed to pattern various patches of alkaline phosphatase linked streptavidin (APLS) (Molecular Probes), which was done from a solution containing 0.1 mg/mL APLS and 1.9 mg/mL fibrinogen. The enzyme containing solution was injected and rinsed out with PBS after less than 1 minute. The immobilized enzyme was used to dephosphorylate the substrate molecule, 4-methylumbelliferyl phosphate (MUP). MUP was chosen because it is only weakly fluorescent, but becomes strongly fluorescent in the blue upon dephosphorylation. Experiments were performed with 0.195 mM MUP in pH 9.8 carbonate buffer (150 mM). The molecule was flowed into the enzyme-containing channels using a modified syringe pump fitted with 100 μL syringes (Hamilton) via Teflon lines. Enzyme turnover was monitored by epifluorescence under the E800 microscope.

Immobilized 2 Enzyme Assay. Using the same laser scanning procedure described above, B4F was again patterned in patches inside fibrinogen coated microchannels. Glucose oxidase linked avidin (GOLA) (Vector Labs) and horseradish peroxidase linked streptavidin (HRPLS) (Molecular Probes) were immobilized either sequentially (2 patches) or in the same patch. GOLA was prepared in PBS at 0.025 mg/mL in a solution also containing 2.7 mg/mL fibrinogen. On the other hand, 0.020 mg/mL HRPLS was immobilized from a solution that contained 2.7 mg/mL fibrinogen in PBS. When GOLA and HRPLS were patterned together as one patch, 100 μL of each solution was added to 800 μL of 3 mg/mL fibrinogen and roughly 200 μL of the mixture was injected into the microchannel. In all cases, enzymes were allowed no more than one minute to bind to the biotin presenting surfaces before being washed out with buffer. This was done to minimize non-specific adsorption.

Glucose oxidase catalyzes the conversion of β-D-glucose and O_2 to gluconolactone and releases H_2O_2. The peroxide can combine with Amplex Red (Molecular Probes) in the active site of horseradish peroxidase to produce resorufin, which is highly fluorescent. A stock solution of Amplex Red was prepared by dissolving 5 mg of the molecule in 0.5 mL of DMSO. The final solution injected into the microchannels was prepared by mixing 1 μL of stock Amplex Red and ~ 1 mg β-D-glucose (Sigma) into 1 mL of PBS. This solution was flowed into the channel and enzyme turnover was monitored via epifluorescence microscopy.

Results

  Streptavidin Immobilization Assay. The binding of B4F to BSA, fibrinogen, IgG, and lysozyme coated channels was investigated in a first set of experiments. Figure 18 shows data from a 12 microchannel PDMS/glass device. From left to right the channels were first incubated with 3 concentrations each of BSA, lysozyme, fibrinogen and IgG, respectively. The fluorescence emanated from Alexa 594 labeled streptavidin that was subsequently flowed over the surface after B4F attachment and allowed to bind to the biotin moieties. A linescan across the patterned area (blue) reveals that the fibrinogen coating led to the greatest density of specifically bound streptavidin molecules and the lowest non-specific adsorption (red). Lysozyme and BSA yielded comparatively moderate patterning densities and suffered from somewhat more non-specific adsorption. IgG was nearly as good as the fibrinogen, but seemed to have slightly fewer specific binding sites. The amount of binding to any particular protein coated surface probably depended on the number of free amines available at the surface.[103] On the other hand, the prevention of non-specific binding by streptavidin should be related at least in part to a coat protein's ability to spread at the surface and cover the bare glass. Based on the above results, 2.5 mg/mL fibrinogen solutions were chosen for forming the passivation coating in all subsequent photopatterning experiments.
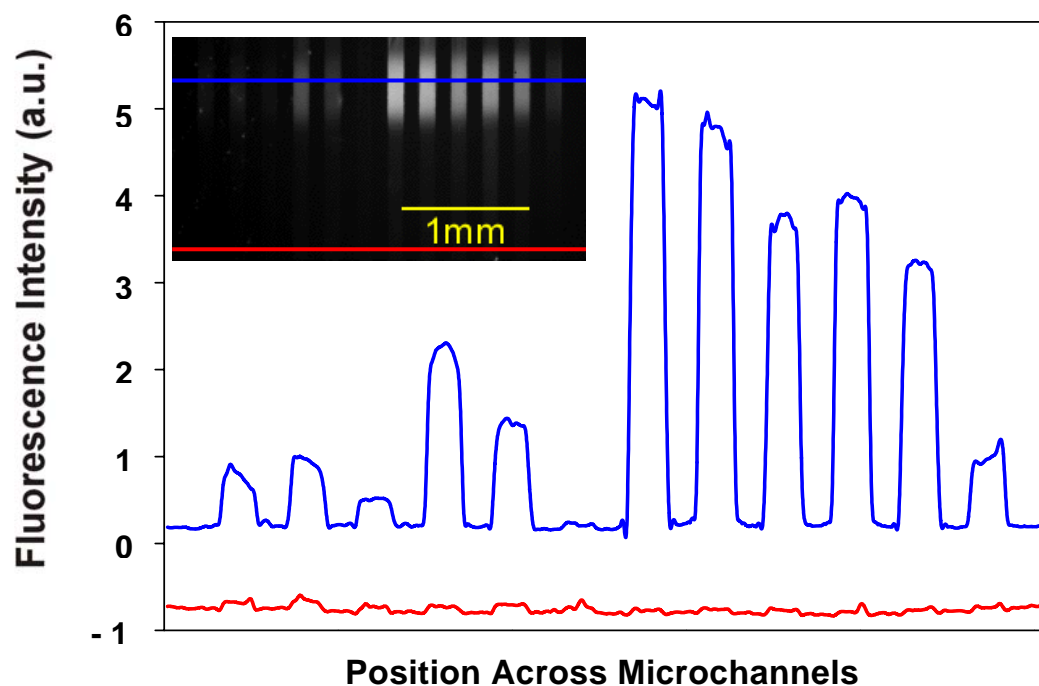
Figure 18. Protein comparison assay. An intensity linescan of fluorescence (blue) emanating from a protein patterned region across a series of microchannels and a second linescan (red) below this (an unpatterned region). The latter was used as a measure of non-specific adsorption. The red and blue scans have been offset by one intensity unit for visual clarity. Channels 1-3 were incubated with BSA at 9.4, 1.8, 0.38 mg/mL respectively, channels 4-6 with lysozyme at 4.1, 0.82, 0.16 mg/mL, channels 7-9 with fibrinogen at 3.0, 0.6, 0.12 mg/mL and channels 10-12 with IgG at 4.4, 0.88, 0.18 mg/mL. Inset: Fluorescence micrograph of the patterned 12 microchannel PDMS/glass array.

Immobilized Single Enzyme Assay. To demonstrate the ability of this process to create well-defined patches of enzyme, APLS was patterned in three parallel microchannels. The first channel contained 1 patch, the second contained two consecutive patches, and the third contained three consecutive patches. Next, MUP was infused into the channels at 20 nL/min and imaged by fluorescence microscopy. A weak background could be observed from all three channels even before the patches because MUP itself is weakly fluorescent. As expected, control experiments verified that this intensity was not flow rate dependent. On the other hand, when the MUP encountered an enzyme patch, the fluorescence signal increased strongly. In the bottom channel there was only a single patch so the increase occurred only once and then leveled off immediately downstream from it (Figure 19). By contrast, two intensity increases could be observed in the middle channel and three from the top channel. In other words, the fluorescence intensity rose as the substrate passed over each subsequent enzyme patch. To determine the fluorescence signal from fully equilibrated substrate, the pump was stopped and the fluorescence was monitored directly over any given patch. Eventually, a maximum intensity was achieved and is represented by the dotted line at the top of the graph in Figure 19. From the single patch data it can be seen that approximately 31% conversion was achieved at a flow of 20 nL/min. Each subsequent downstream patch turns over less substrate, because there was a lower concentration of it left to convert. Approximately 67% of the maximum substrate turnover could be achieved after three patches. It was possible to speed up or slow down the flow rate to modulate the
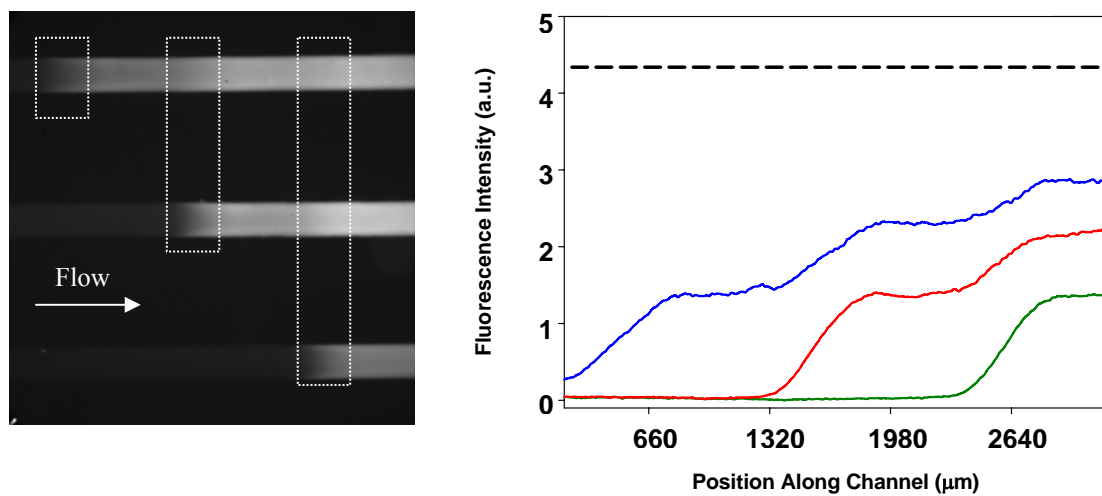
Figure 19. Multipattern single enzyme assay. Left: fluorescence micrograph (3.2 x 3.2 mm) of a 3 channel PDMS/glass device patterned with APLS. The top channel has 3 patches, the middle has 2 patches and the bottom has 1 patch. The patch positions are outlined with white rectangles. Right: Fluorescence linescans along each individual channel (blue top, red middle and green bottom). The dashed line represents the maximum product intensity achieved in the microchannels when the flow was stopped.

fluorescence intensity jumps; however, it should be noted that below 20 nL/min, the flow rate became uneven in the present setup. This was caused by slip-stick friction in the individual syringes. It is also of importance to note the ease with which consecutive patch geometries can be achieved. This is often difficult to accomplish with other immobilization strategies.

To obtain more quantitative information from the reactor, it was necessary to estimate the number density of immobilized APLS enzymes in a given patch. Control experiments were performed with streptavidin, which has a roughly 33.6 nm^2 footprint on a membrane surface.[104] Known densities, 3 x 10^4 streptavidin molecules/μm, of this protein were bound to biotinylated supported lipid bilayers following our previously reported procedures.[34] By comparison of those results with the present experiments, it was revealed that streptavidin coverage could reach approximately 5% of the close packed density for photoattachment to fibrinogen. Since the area of a patch was at most 0.8 mm x 0.29 mm, this meant that no more than 7 x 10^8 streptavidin molecules were bound to the channel walls under the conditions described above. It is reasonable to assume that immobilized APLS would have approximately the same number density as streptavidin alone since the distance between the surface attached species was quite large compared to the average footprint size for this linked protein complex (134 nm^2).[34]

At a flow rate of 20 nL/min, it should take a substrate molecule roughly 4.2 seconds to cross a 0.8 mm patch. From the data in Figure 19, the first patch of each channel converted ~31% of substrate to product. Employing a substrate concentration of 0.195 mM, we found that 5.13 x 10^{10} molecules of substrate were converted by 7 x 10^8

AP enzymes in 4.2 seconds to yield a turnover number of ~20 molecules per enzyme per second. Several assumptions were made in this estimation of turnover number, (1) the top and bottom of the channel contained the same enzyme density, (2) every site of patterned biotin was available for enzyme binding, (3) the cross sectional area of the PDMS/glass device was constant, and (4) the enzymes were uniformly patterned. Such assumptions lead to a lower bound to the actual turnover rate. The AP patch enzyme reactor was very robust and capable of operating for a minimum of several hours of continuous substrate turnover. In fact, one APLS reactor was kept hydrated at room temperature for 2 days and when substrate was reintroduced, the turnover rate was more than 90% of the initial value.

Immobilized Two Enzyme Assay. Using the methodology described above, we sequentially patterned glucose oxidase and horseradish peroxidase in a single microchannel to perform a two-step enzyme reaction. HRPLS and GOLA were patterned such that the horseradish peroxidase was downstream from the glucose oxidase. In the first step, GOLA oxidized glucose to form gluconolactone and hydrogen peroxide. Next, the peroxide combined at the active site of HRPLS with Amplex Red to form resorufin, which fluoresces strongly near 580 nm upon excitation with green light. Amplex Red was prepared in PBS buffer with β-D-glucose as described in the experimental section. It was found that sufficient oxygen was already dissolved in PBS just from exposure to ambient air; therefore, it was not necessary to purge with additional oxygen.

The substrate was pumped into the device at 50 nL/min and the fluorescence intensity jumped dramatically after the HRPLS patch, as can be clearly seen from the image and accompanying line profile (blue line, Figure 20a). It should be noted, however, that there was already a small rise in intensity[105] directly before the HRPLS patch (red line, Figure 20a). In fact, 6.7% of the ultimate fluorescence intensity was achieved before the second patch. This was the case because HRPLS suffers from a relatively high degree of non-specific adsorption. H_2O_2 is produced as soon as the GOLA patch is encountered. Amplex Red is, therefore, turned over by even minute quantities of HRPLS that are non-specifically adsorbed downstream from this location. The reason for the non-specific adsorption problem almost certainly stems from the fact that horseradish peroxidase has a pI very close to neutral pH (7.2). This can potentially lead to aggregation and surface adsorption problems when patterning the protein from standard buffer solutions. To reduce this interaction, the HRPLS photopatterning was repeated (data not shown), at a pH of 9.8. This reduced the background to 4.5% of the ultimate turnover before the final patch under the same conditions.

In an effort to lower the background turnover even further, a separate experiment was performed with an equimolar mixture of GOLA and HRPLS patterned together in the same patch at pH 7.2 (Figure 20b). The background was reduced to 2.2% of the eventual total turnover, meaning that some nonspecific adsorption of both enzymes was occurring before the patch.
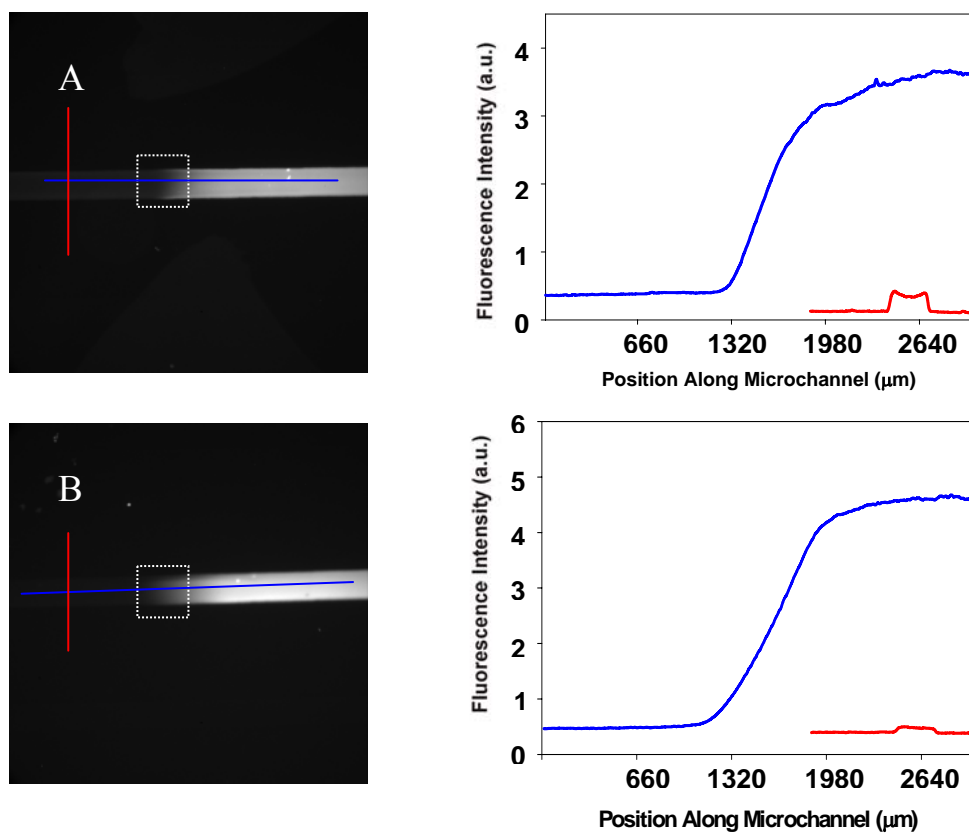
Figure 20. Two enzyme reactor. Left: fluorescence images of PDMS/glass microchannel devices patterned with GOLA and HRPLS imaged near the HRPLS patch (boxes). (a) A sequentially patterned enzyme channel and (b) a single patch with both enzymes placed in the same location. Right: The blue lines represent the product intensities along the channels. The red lines show the background intensity taken across the microchannels approximately 1 mm before the final enzyme patch. The flow rate was 50 nL/min in both reactors.

Discussion

The enzyme immobilization method presented herein has several advantages over previous enzyme reactors. The method is general, allows precise control over enzyme placement, and could be used in conjunction with virtually any microfluidic geometry. Patterning enzymes requires no UV irradiation[62,88,89,91] and is quite fast. Furthermore, patterning can be done from an aqueous solution without ever exposing the protein molecules to air,[106,107] which should help maintain their integrity, although this was not a major concern with rugged enzymes such as alkaline phosphatase, horse radish peroxidase, or glucose oxidase. More than one enzyme can be patterned in a single straight channel to run multi-step reactions without valves or additional complexities.

There are also some disadvantages to the present strategy. For example, this patterning process relies on a biotin-streptavidin linkage, which limits flexibility. While it is relatively easy to biotinylate almost any protein with commercially available linking kits, some enzymes may be more sensitive to environmental conditions of pH, ionic strength, and temperature. This could lead to the loss of activity under linking conditions. There may, of course, be ways around this. Indeed, we have previously shown that the photoattachment process works for a variety of fluorophore dyes,[101] and it should be possible to create functionalized dyes which can be used to directly capture proteins from solution using specific chemistry. For example, maleimido groups tethered to dyes are typically used to label cysteine residues. It should therefore be possible to photoattach dyes to create patches of maleimido groups, which could subsequently react with free cysteines on the surface of engineered proteins. The

sulfhydryl reaction chemistry could provide a generic linking chemistry for capturing novel enzymes for study in such systems. Also, by combining a variety of fluorophores, which photobleach at different wavelengths, with antibody specific ligands, it should be possible to create more complicated sequences of antibody-linked enzymes simultaneously, rather than sequentially.

Another concern in these experiments was the non-specific adsorption of the HRPLS and GOLA enzymes. This caused some background fluorescence before the enzyme patch, whether patterned separately or together. This background level may be acceptable in the framework of combinatorial analysis since sharp changes in enzyme activity can be easily recorded in parallel. Applications requiring < 1% background, however, need to be optimized by varying salt concentration, surface chemistry and solution additives to minimize the non-specific problem. Further experiments will be needed to explore this issue and the particular strategy employed may ultimately depend on the particular enzyme which is being patterned.

Conclusion

We have developed a basic strategy for the photo-immobilization of multiple, well-defined enzyme patches in simple PDMS/glass microfluidic channels. This method allowed us to estimate enzyme turnover number for a single enzyme system. The technique also proved to be viable for multi-step enzyme reactions by patterning proteins in sequence. Non-specific adsorption of enzymes was reduced by careful selection of the surface passivating layer and by adding competitive non-specific adsorbers to the patterning solutions.

CHAPTER VII

PRESERVED SOLID SUPPORTED BILAYERS

Introduction

Solid supported lipid bilayers[108-110] possess a unique combination of physical

properties, which make them well suited to serve as cell membrane mimics.[111,112] Chief

among these is the two-dimensional fluidity of the individual lipid molecules.[113-115] Such

mobility is crucial for studies of cell signaling, pathogen attack, trafficking of

lymphocytes, as well as the inflammatory response.[116-118] Mobility is required because

all these processes involve multivalent ligand-receptor attachment, which relies on the

reorganization of cell surface constituents.[119-123]

When fully hydrated, supported lipid bilayers can be employed as sensor

platforms; however, these systems are quickly destroyed upon exposure to the air/water

interface,[22] and therefore must remain underwater at all times. Several attempts have

been made to overcome this limitation. Hybrid bilayers,[24] with a bottom leaflet

consisting of a self-assembled thiol monolayer on gold and a top leaflet of lipids can be

prepared in air and then hydrated without substantially damaging the bilayer.[124]

However, at best, only the top leaflet is laterally mobile, and this mobility is likely

reduced in comparison to full bilayers. Cross-linked bilayers prepared by

photopolymerization of synthetic lipids also produce air-stable membranes, but with

very low lateral mobility.[23,125,126] Furthermore, glass modified with γ-aminopropylsilane

has been used as a substrate for bilayers that could be dried and rehydrated.[25] These

bilayers possessed some long range lateral mobility as observed by fluorescence

recovery after photobleaching (FRAP). However, the degree of recovery was only 50% even before drying, whereas glass supported bilayers typically recover more than 90% of their original fluorescence intensity.[127,128] It would be highly desirable to create solid supported bilayers which could be insensitive to the air/water interface, yet still maintain complete fluidity. In addition, if these bilayers could be dried and stored, it would substantially increase their utility as sensing platforms.

Chapter VII describes a novel method by which solid supported lipid bilayers can be dried and preserved via specifically bound proteins. The intrinsic property of lateral lipid mobility was maintained during this process, which was examined in two distinct scenarios. First, bilayers with a dense monolayer of specifically bound protein could be drawn repeatedly through the air/water interface without damaging the bilayer. Bulk water was seen to cling to the protein on the bilayer, thereby shielding the bilayer from air. Second, the protein-bound bilayer was intentionally dried under a stream of nitrogen, which removed all bulk water. Not only was the bilayer still in tact, but when placed in a humid environment, the lateral mobility of the individual lipids was visible by fluorescence photobleaching recovery.

Experimental

Microfluidics. Small wells were created by reaming 8 mm holes through PDMS slabs and subsequently pressing the nascent mold against clean glass coverslips. The four channel PDMS mold was prepared by photolithography. Briefly, SU-8 photoresist was spun onto a silicon wafer to a thickness of 20 microns and exposed through a photomask using a mask aligner. The final channels were 800 microns by 1 cm. Inlet

and outlet holes were reamed with a flat-tipped syringe needle. The channels were adsorbed to clean microscope coverslips and solutions were injected gently so as not to break the seal with the glass.

Preparation of Bilayer Vesicles and Supported Bilayers. Small unilamellar vesicles were prepared as previously reported.[129,130] Briefly, lipids were dissolved in chloroform and allowed to dry under a stream of nitrogen followed by desiccation under vacuum for 2 h. The lipids were reconstituted in PBS buffer (pH 7.2) and extruded more than seven times through polycarbonate filters with 50 nm pores. Upon injection into a microfluidic device, the lipid vesicles spontaneously fused to the glass to form a continuous planar lipid bilayer. Excess vesicles were flushed away with pure buffer. The quality of the supported bilayers on the glass surface was verified by fluorescence recovery after photobleaching (FRAP). The supported bilayer used in these experiments was 94% egg phosphatidylcholine (egg PC; Avanti Polar Lipids, Alabaster, AL), 1% Texas-Red dihexadecanoyl-phosphatidylethanolamine (TR-DHPE) (Molecular Probes, Eugene, OR) and 5% (or lower) biotin-linked phosphatidylethanolamine (biotin-PE). It was assumed in all studies that the concentrations of ligand in the upper and lower leaflets of the bilayer were similar.

Conditions for Humid FRAP. Bilayers formed on clean microscope coverslips using the PDMS well were rinsed with PBS to remove excess vesicles and then incubated with 0.025mg/ml streptavidin. This was subsequently rinsed with more PBS. About half of the buffer was then removed and the PDMS well was carefully peeled from the glass, such that a dome of buffer remained on top of the bilayer. A stream of

nitrogen was used to quickly remove this bulk water, which usually took 1-2 seconds. The glass coverslip was inverted and one edge was adsorbed to a piece of PDMS as a holder. This assembly was placed into a Petri dish and the dish mounted on the stage of a Nikon E800 microscope. Since the objective (40X) used had a very short working distance, the spot was bleached in ambient air with the lid of the Petri dish off. After bleaching, the lid was replaced, and FRAP was monitored with a 10X objective. The dish had a small hole in the side, into which 4 mL of water was injected. As this water evaporated, a humid environment was created inside the covered Petri dish, thereby allowing bilayer to recover.

Results and Discussion

Solid supported bilayers were prepared by fusing vesicles containing 5% biotin-linked phosphatidylethanolamine (biotin-PE), 1% Texas-Red dihexadecanoyl-phosphatidylethanolamine (TR-DHPE) and 94% egg phosphatidylcholine (egg-PC) to a four channel polydimethylsiloxane/glass microfluidic device. Every other supported bilayer was incubated with a solution of 0.25 mg/mL streptavidin in pH 7.2 PBS and then rinsed with PBS. While under water, the PDMS channels were peeled off the glass and the bilayers imaged (Figure 21a). The sample was then drawn through the air/water interface 5 times and re-imaged under water. Figure 21b clearly shows that the bilayers bound with streptavidin were still present, while the unprotected bilayers were completely removed. FRAP measurements revealed that drawing the sample through the air/water interface did not reduce the lateral lipid mobility.

Through air/water interface 5X
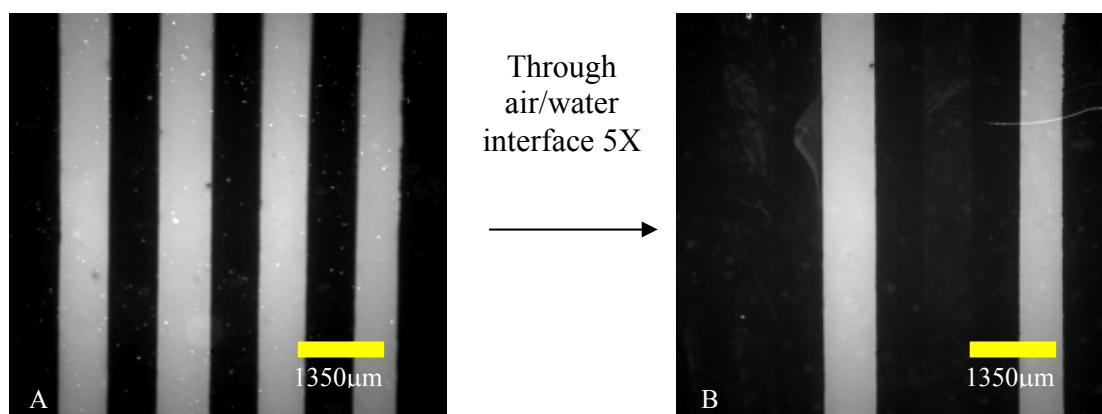
Figure 21. Protein vs. no protein. (a) A fluorescence micrograph image of four 5% biotin-PE, 1% TR-DHPE, 94% egg-PC bilayers formed inside microfluidic channel (left). The second and fourth from the left were saturated with bound streptavidin. (b) Same system drawn 5X through the air/water interface. The bilayers with streptavidin remained intact while those without protein were destroyed.

When drawn through the interface, a thin layer of water was clearly visible over the lanes which were protected with streptavidin. This water layer clung tenaciously; therefore, during the withdrawal and re-immersion cycles, bulk water was constantly present.

In a separate experiment, bilayers containing the same constituents as above were prepared on glass, bound with streptavidin and rinsed with PBS. At this point, the sample was dried under a stream of N_2. Remarkably, the entire bilayer was still present and in excellent condition as seen by fluorescence microscopy. An 80 μm diameter spot was bleached on this bilayer while in air, but did not recover. However, when the sample was placed in a high humidity environment the bleached spot recovered 93% of its initial fluorescence intensity. Figure 22 shows fluorescence micrographs of two bleached and recovered spots, as well as the FRAP curve for one of them as a function of time. The recovery time was used to calculate the diffusion coefficient of the lipids in humid air of 8 x 10^{-10} cm^2/sec, which is two orders of magnitude slower than the diffusion under water.

Effect of Ligand Density on Bilayer Preservation. We prepared four bilayers using the PDMS channels, each of which had a successively higher concentration of ligand. All channels were incubated with the same 0.025 mg/mL streptavidin solution. Figure 23 shows the bilayers before and after drawing through the air/water interface. From left to right, the ligand density was 4, 3, 2 and 1%. From the images, the bilayers with below 3% ligand density began to show significant damage. We have previously

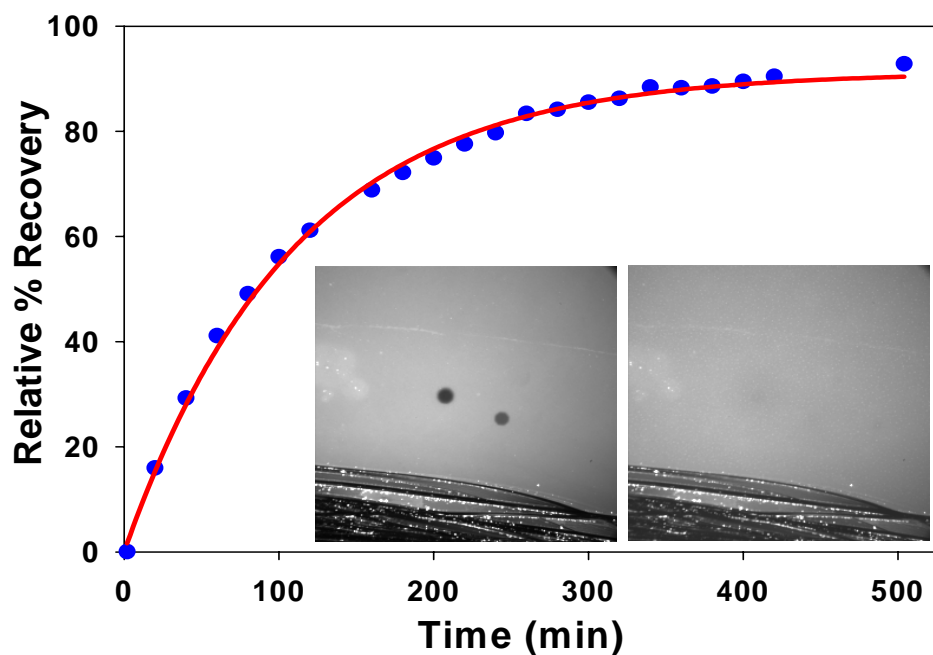**Figure 22.** Air FRAP. The left image (inset) shows two bleached spots made while the dried bilayer was in ambient air. The sample recovered 93% of its initial fluorescence intensity when placed in a humid chamber (inset right). Scratches at the bottom of each image were intentionally made with metal tweezers for background estimation. The curve was obtained from the FRAP of the upper left spot, which was bleached more fully.
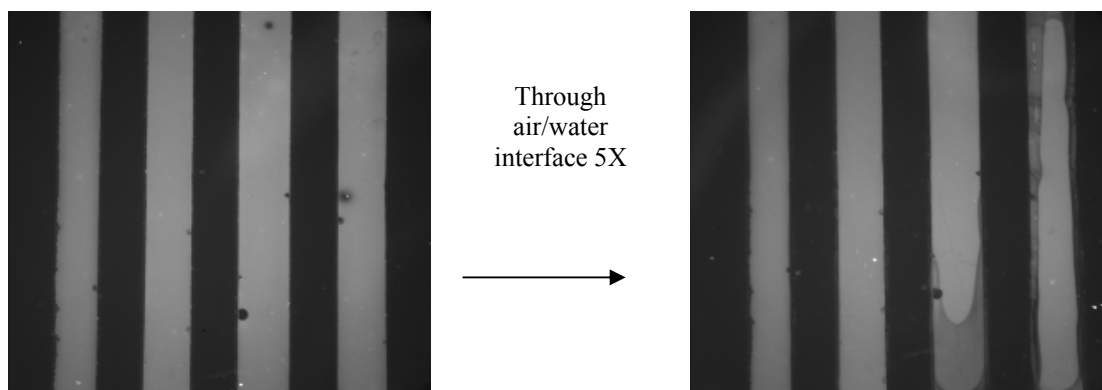
Through
air/water
interface 5X

Figure 23. Effect of ligand density on bilayer protection. From left to right, the ligand concentration is 4, 3, 2, and 1% in the 1% Texas Red bilayer. Note that the edges of the 2 and 1% lanes become damaged upon drawing through the air/water interface.

shown that the streptavidin surface coverage saturates at 3% biotin density. Therefore, the protecting property of the protein is maximized at full coverage.

While the exact mechanism of how the protein protects bilayers from destruction is still unknown, two factors are considered here. First, the close packing of the specifically bound streptavidin monolayer (Figure 24) may stiffen the bending elastic modulus of the bilayer.[131]   A separate experiment was performed to examine the effect of ligand density vs. streptavidin protection. At low biotin densities significant damage was done to the bilayer upon drawing through the air/water interface (see Supporting Info) and the effect of the protein layer is probably maximized at full coverage. We have repeated this experiment with other bound proteins such as IgGs and it seems that the protein's identity is not the crucial factor. A mechanism involving a change in the bending modulus would be reminiscent of the forces which lead to the formation of inside-out vesicles when Escherichia Coli are forced through a French press.[132-134] Proteins, normally on the inside of the bacteria, relocate to the outside of the smaller vesicle membranes, presumably due to the mechanical and electrostatic forces between the surface membrane proteins. Similar forces may serve to stabilize these supported bilayers during nitrogen drying.

Second, it should be noted that in the absence of a protein layer one might expect the lipid molecules in dry bilayers to reorganize to have their alkyl chains point toward the air. This destructive effect is apparently avoided by the presence of the protein layer.
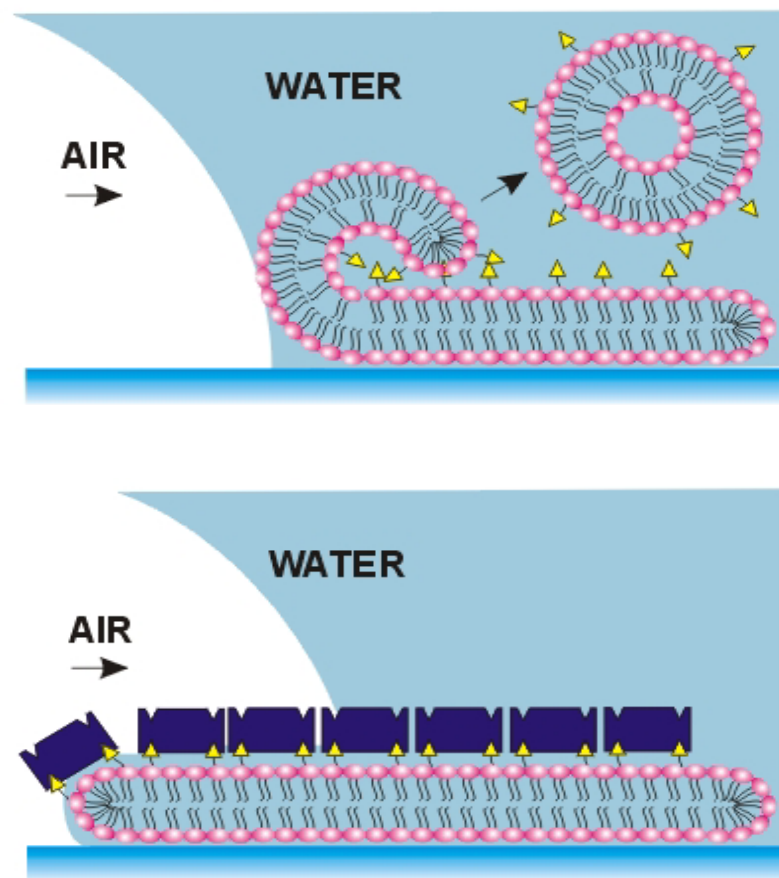
Figure 24. Suggested protection mechanism. (top) The introduction of the air/water interface destroys the bilayer from the edge, peeling the membrane away in vesicle sections. When the same bilayer is protected by a close-packed protein monolayer (bottom), it survives the air/water interface. The proteins may serve to mechanically "pin" down the edge of the bilayer, allowing air to flow over the surface without disrupting the overall lipid ordering. Also, a thin layer of water is trapped between the protein and the bilayer, while bulk water is removed with a nitrogen stream.

Indeed, a thin layer of water which is likely bound to the protein-coated bilayers, thereby keeping the system partially hydrated even when blown dry with a stream of nitrogen.

Therefore, though the bulk water is removed very quickly, surface-bound water, including water which may penetrate slightly into the membrane, remains behind. This water may later evaporate under sufficiently low humidity conditions, leaving the bilayer mostly dehydrated, but still in tact because of the difficulty of reorganizing the alkyl chains in the presence of the protein. The fact that the bilayer could not recover in ambient air, but could recover in humid air, supports this possibility. Namely, the presence of some interfacial water molecules imparts fluidity.

Conclusion

This method of bilayer preservation requires no substrate modification and can be performed using commercially available reagents. The bilayer retains its property of lateral fluidity, even when removed from bulk water. This has potentially important implications in the field of biosensing, where rugged sensors which can approximate the complex processes of multivalent recognition would be crucial for detecting biological agents. If fluid bilayers could be preserved and stored for later rehydration, complex sensor arrays could be manufactured at dedicated facilities and then later employed in the field. Another tantalizing possibility is the use of this method to preserve black lipid membranes. Traditionally, these are very delicate systems, which, in combination with single ion channels extracted from cell membranes, can serve as specific single molecule sensors.[135] Adding a monolayer of specifically bound protein could potentially strengthen BLM's to create rugged single molecule sensor platforms.[136-138]

CHAPTER VIII

SUMMARY

A microfluidic device was created for the generation of concentration gradients. The process worked by combining two flowing streams at a Y junction and allowing the dissolved analytes to interdiffuse as a function of distance and linear fluid velocity. Gradients could be maintained as long as the flow was constant and could range over 3 orders of magnitude. This system could be employed for combinatorial concentration dependent measurements.[34,53] Next, bleached fluorophores were found to rapidly attach to electron rich surfaces, thereby creating a new visible light patterning method. Patches of biotin-4-fluorescein, a ligand-linked dye, were patterned using this process inside microfluidic channels. Avidin or streptavidin linked enzymes were subsequently immobilized at the biotin sites, and substrate turnover was monitored by infusing substrate at a known speed and recording fluorogenic cleavage. This immobilization chemistry was fully compatible with aqueous solution, and worked at variety of wavelengths, depending on the fluorophore's resonance. Finally, a new method for supported bilayer preservation was explored. Proteins specifically bound to ligands tethered to the supported membrane provided protection from the air/water interface. This was verified by the fact that FRAP was still possible even without the presence of bulk water (i.e. in humid air). Such bilayers showed the possibility for long term storage and rehydration for future use.

REFERENCES

(1) Rusling, J. F. *Biomolecular films: Design, function, and applications*; Marcel

Dekker: New York, 2003.

(2) Prince, L. M.; Sears, D. F. *Biological horizons in surface science*; Academic Press:

New York, 1973.

(3) Baszkin, A.; Norde, W. *Physical chemistry of biological interfaces*; Marcel Dekker:

New York, 2000.

(4) Huber, B. T.; Palmer, E. *Superantigens: A pathogen's view of the immune system*;

Cold Spring Harbor Laboratory Press: Plainview, NY, 1993.

(5) Poste, G.; Nicolson, G. L. *Virus infection and the cell surface*; North Holland Pub

Co.: New York, 1977.

(6) Brash, J. L. *Proteins at interfaces II: Fundamentals and applications*; American

Chemical Society: Washington, DC, 1995.

(7) Wardle, E. N. *Cell surface science in medicine and pathology*; Elsevier Science Pub.

Co.: New York, 1985.

(8) Bradshaw, R. A.; Dennis, E. A. *Handbook of cell signaling*; Academic Press:

Boston, 2004.

(9) Weigl, B. H.; Yager, P. *Science* **1999**, *283*, 346-347.

(10) Hatch, A.; Kamholz, A. E.; Hawkins, K. R.; Munson, M. S.; Schilling, E. A.;

Weigl, B. H.; Yager, P. *Nat. Biotechnol.* **2001**, *19*, 461-465.

(11) Kenis, P. J. A.; Ismagilov, R. F.; Takayama, S.; Whitesides, G. M.; Li, S. L.;

White, H. S. *Acc. Chem. Res.* **2000**, *33*, 841-847.

(12) Kenis, P. J. A.; Ismagilov, R. F.; Whitesides, G. M. *Science* **1999**, *285*, 83-85.

(13) Xia, Y. N.; Whitesides, G. M. *Angew. Chem. Int. Ed. Engl.* **1998**, *37*, 551-575.

(14) Jona, G.; Snyder, M. *Curr. Opin. Mol. Therapeutics* **2003**, *5*, 271-277.

(15) Huang, R. P. *Front. Biosci.* **2003**, *8*, D559-D576.

(16) Frank, R. *Comb. Chem. High Throughput Screen* **2002**, *5*, 429-440.

(17) Smyth, G. K.; Speed, T. *Methods* **2003**, *31*, 265-273.

(18) Reese, M. O.; van Dam, R. M.; Scherer, A.; Quake, S. R. *Genome Res.* **2003**, *13*, 2348-2352.

(19) Heller, M. J. *Annu. Rev. Biomed. Eng.* **2002**, *4*, 129-153.

(20) Fodor, S. P. A. *Science* **1997**, *278*, 1551-1551.

(21) Tien, H. T.; Ottova-Leitmannova, A. *Planar lipid bilayers (BLMs) and their applications*; Elsevier: Amsterdam, 2003.

(22) Cremer, P. S.; Boxer, S. G. *J. Phys. Chem. B* **1999**, *103*, 2554-2559.

(23) Ross, E. E.; Bondurant, B.; Spratt, T.; Conboy, J. C.; O'Brien, D. F.; Saavedra, S. S. *Langmuir* **2001**, *17*, 2305-2307.

(24) Plant, A. L. *Langmuir* **1999**, *15*, 5128-5135.

(25) Fang, Y.; Frutos, A. G.; Lahiri, J. *J. Am. Chem. Soc.* **2002**, *124*, 2394-2395.

(26) Lin, C. H.; Lee, G. B.; Lin, Y. H.; Chang, G. L. *J. Micromech. Microeng.* **2001**, *11*, 726-732.

(27) Beebe, D. J.; Moore, J. S.; Bauer, J. M.; Yu, Q.; Liu, R. H.; Devadoss, C.; Jo, B. *Nature* **2000**, *404*, 588-590.

(28) Duffy, D. C.; Schueller, O. J. A.; Brittain, S. T.; Whitesides, G. M. *J. Micromech. Microeng.* **1999**, *9*, 211-217.

(29) Hosokawa, K.; Fujii, T.; Endo, I. *Anal. Chem.* **1999**, *71*, 4781-4785.

(30) Lemmo, A. V.; Fisher, J. T.; Geysen, H. M.; Rose, D. J. *Anal. Chem.* **1997**, *69*, 543-551.

(31) Unger, M. A.; Chou, H.; Thorsen, T.; Scherer, A.; Quake, S. R. *Science* **2000**, *288*, 113-116.

(32) Yang, T.; Jung, S. Y.; Mao, H.; Cremer, P. S. *Anal. Chem.* **2001**, *73*, 165-169.

(33) Yang, T.; Simanek, E. E.; Cremer, P. S. *Anal. Chem.* **2000**, *72*, 2587-2589.

(34) Mao, H.; Yang, T.; Cremer, P. S. *Anal. Chem.* **2002**, *74*, 379 -385.

(35) Henry, A. C.; Tutt, T. J.; Galloway, M.; Davidson, Y. Y.; McWhorter, C. S.; Soper, S. A.; McCarley, R. L. *Anal. Chem.* **2000**, *72*, 5331-5337.

(36) Barker, S. L.; Ross, D.; Tarlov, M. J.; Gaitan, M.; Locascio, L. E. *Anal. Chem.* **2000**, *72*, 5925-5929.

(37) Zhao, B.; Moore, J. S.; Beebe, D. J. *Science* **2001**, *291*, 1023-1026.

(38) Duffy, D. C.; Gillis, H. L.; Lin, J.; Sheppard, N. F. J.; Kellogg, G. J. *Anal. Chem.* **1999**, *71*, 4669-4678.

(39) Culbertson, C. T.; Jacobson, S. C.; Ramsey, J. M. *Anal. Chem.* **2000**, *72*, 5814-5819.

(40) Jacobson, S. C.; McKnight, T. E.; Ramsey, J. M. *Anal. Chem.* **1999**, *71*, 4455-4459.

(41) Jeon, N. L.; Dertinger, K. W.; Chiu, D. T.; Choi, I. S.; Stroock, A. D.; Whitesides, G. M. *Langmuir* **2000**, *16*, 8311-8316.

(42) Dertinger, S. K.; Chiu, D. T.; Jeon, N. L.; Whitesides, G. M. *Anal. Chem.* **2001**, *73*, 1240-1246.

(43) Anderson, J. R.; Chiu, D. T.; Jackman, R. J.; Cherniavskaya, O.; McDonald, J. C.; Wu, H.; Whitesides, S. H.; Whitesides, G. M. *Anal. Chem.* **2000**, *72*, 3158-3164.

(44) Chiu, D. T.; Jeon, N. L.; Huang, S.; Kane, R. S.; Wargo, C. J.; Choi, I. S.; Ingber, D. E.; Whitesides, G. M. *Proc. Natl. Acad. Sci. USA* **2000**, *97*, 2408-2413.

(45) Takayama, S.; McDonald, J. C.; Ostuni, E.; Liang, M. N.; Kenis, P. J. A.; Ismagilov, R. F.; Whitesides, G. M. *Proc. Natl. Acad. Sci. USA* **1999**, *96*, 5545-5548.

(46) Kamholz, A. E.; Weigl, B. H.; Finlayson, B. A.; Yager, P. *Anal. Chem.* **1999**, *71*, 5340-5347.

(47) Bessoth, F. G.; deMello, A. J.; Manz, A. *Anal. Comm.* **1999**, *36*, 213-215.

(48) Kamholz, A. E.; Yager, P. *Sens. Actuators B* **2002**, *82*, 117-121.

(49) Ismagilov, R. F.; Stroock, A. D.; Kenis, P. J. A.; Whitesides, G.; Stone, H. A. *Appl. Phys. Lett.* **2000**, *76*, 2376-2378.

(50) Beskok, A.; Warburton, T. C. E. *J. Comput. Phys.* **2001**, *174*, 492-509.

(51) Kumar, S. *Numerical Simulation of Microfluidic Passive and Active Mixers*; M.S. Thesis, Texas A&M University: College Station, 2002.

(52) Fan, Z. H.; Harrison, D. J. *Anal. Chem.* **1994**, *66*, 177-184.

(53) Mao, H.; Holden, M. A.; Yu, M.; Cremer, P. S. *Anal. Chem.* **2002**, *5071-5075*.

(54) Ocvirk, G.; Munroe, M.; Tang, T.; Oleschuk, R.; Westra, K.; Harrison, D. J. *Electrophoresis* **2000**, *21*, 107-115.

(55) Chen, X. X.; Wu, H. K.; Mao, C. D.; Whitesides, G. M. *Anal. Chem.* **2002**, *74*, 1772-1778.

(56) Eteshola, E.; Leckband, D. *Sens. Actuators B* **2001**, *72*, 129-133.

(57) Eon, D.; de Poucques, L.; Peignon, M. C.; Cardinaud, C.; Turban, G.; Tserepi, A.; Cordoyiannis, G.; Valamontes, E. S.; Raptis, I.; Gogolides, E. *Microelec. Eng.* **2002**, *61* (2), 901-906.

(58) Abbasi, F.; Mirzadeh, H.; Katbab, A. A. *Polymer. Int.* **2001**, *50*, 1279-1287.

(59) Delamarche, E.; Schmid, H.; Michel, B.; Biebuyck, H. *Adv. Mater.* **1997**, *9*, 741-746.

(60) Monahan, J.; Gewirth, A. A.; Nuzzo, R. G. *Anal. Chem.* **2001**, *73*, 3193-3197.

(61) Willner, I.; Katz, E. *Angew. Chem. Int. Ed.* **2000**, *39*, 1180-1218.

(62) Blawas, A. S.; Reichert, W. M. *Biomaterials* **1998**, *19*, 595-609.

(63) Nivens, D. A.; Conrad, D. W. *Langmuir* **2002**, *18*, 499-504.

(64) Matsuda, T.; Sugawara, T. *Langmuir* **1995**, *11*, 2272-2276.

(65) Matsuda, T.; Sugawara, T. *Langmuir* **1995**, *11*, 2267-2271.

(66) Deng, L.; Mrksich, M.; Whitesides, G. M. *J. Am. Chem. Soc.* **1996**, *118*, 5136-5137.

(67) Harder, P.; Grunze, M.; Dahint, R.; Whitesides, G. M.; Laibinis, P. E. *J. Phys. Chem. B* **1998**, *102*, 426-436.

(68) Holmlin, R. E.; Chen, X. X.; Chapman, R. G.; Takayama, S.; Whitesides, G. M. *Langmuir* **2001**, *17*, 2841-2850.

(69) Ostuni, E.; Chapman, R. G.; Liang, M. N.; Meluleni, G.; Pier, G.; Ingber, D. E.; Whitesides, G. M. *Langmuir* **2001**, *17*, 6336-6343.

(70) Chen, G. P.; Ito, Y.; Imanishi, Y.; Magnani, A.; Lamponi, S.; Barbucci, R. *Bioconj. Chem.* **1997**, *8*, 730-734.

(71) Ito, Y.; Chen, G. P.; Imanishi, Y. *Biotechnol. Prog.* **1996**, *12*, 700-702.

(72) Yan, M. D.; Cai, S. X.; Wybourne, M. N.; Keana, J. F. W. *J. Am. Chem. Soc.* **1993**, *115*, 814-816.

(73) Caelen, I.; Gao, H.; Sigrist, H. *Langmuir* **2002**, *18*, 2463-2467.

(74) Wessa, T.; Rapp, M.; Sigrist, H. *Colloids Surf. B* **1999**, *15*, 139-146.

(75) Chevolot, Y.; Bucher, O.; Leonard, D.; Mathieu, H. J.; Sigrist, H. *Bioconj. Chem.* **1999**, *10*, 169-175.

(76) Sanger, M.; Sigrist, H. *Sens. Actuators A* **1995**, *51*, 83-88.

(77) Clemence, J. F.; Ranieri, J. P.; Aebischer, P.; Sigrist, H. *Bioconj. Chem.* **1995**, *6*, 411-417.

(78) Sundarababu, G.; Gao, H.; Sigrist, H. *Photochem. Photobiol.* **1995**, *61*, 540-544.

(79) Delamarche, E.; Sundarababu, G.; Biebuyck, H.; Michel, B.; Gerber, C.; Sigrist, H.; Wolf, H.; Ringsdorf, H.; Xanthopoulos, N.; Mathieu, H. J. *Langmuir* **1996**, *12*, 1997-2006.

(80) Dorman, G.; Prestwich, G. D. *Biochemistry* **1994**, *33*, 5661-5673.

(81) Dorman, G.; Prestwich, G. D. *Trends Biotechnol.* **2000**, *18*, 64-77.

(82) Liu, X. H.; Wang, H. K.; Herron, J. N.; Prestwich, G. D. *Bioconj. Chem.* **2000**, *11*, 755-761.

(83) Rozsnyai, L. F.; Benson, D. R.; Fodor, S. P. A.; Schultz, P. G. *Angew. Chem. Int. Ed.* **1992**, *31*, 759-761.

(84) Nakagawa, M.; Ichimura, K. *Colloids Surf. A* **2002**, *204*, 1-7.

(85) Leipert, D.; Heiduschka, P.; Mack, J.; Egelhaaf, H. J.; Oelkrug, D.; Jung, G. *Angew. Chem. Int. Ed.* **1998**, *37*, 2338-2340.

(86) Fodor, S. P. A.; Read, J. L.; Pirrung, M. C.; Stryer, L.; Lu, A. T.; Solas, D. *Science* **1991**, *251*, 767-773.

(87) Blawas, A. S.; Oliver, T. F.; Pirrung, M. C.; Reichert, W. M. *Langmuir* **1998**, *14*, 4243-4250.

(88) Yang, Z. P.; Frey, W.; Oliver, T.; Chilkoti, A. *Langmuir* **2000**, *16*, 1751-1758.

(89) Pritchard, D. J.; Morgan, H.; Cooper, J. M. *Anal. Chem.* **1995**, *67*, 3605-3607.

(90) Hengsakul, M.; Cass, A. E. G. *Bioconj. Chem.* **1996**, *7*, 249-254.

(91) Dontha, N.; Nowall, W. B.; Kuhr, W. G. *Anal. Chem.* **1997**, *69*, 2619-2625.

(92) Mason, W. T. *Fluorescent and luminescent probes for biological activity : A practical guide to technology for quantitative real-time analysis*; 2nd ed.; Academic Press: San Diego, 1999.

(93) Shaap, P. A. *Singlet molecular oxygen*; Dowden, Hutchinson and Ross: Stroudsburg, PA, 1976.

(94) A deposition process using whole proteins can lead to multilayer formation because nascently photobleached molecules can attach to proteins already patterned on the

surface. This will usually not be the case when small molecules are patterned. In fact, we have demonstrated that patterning biotin-4-fluorescein leads to saturation behavior for streptavidin.

(95) Heo, J.; Thomas, K. J.; Seong, G. H.; Crooks, R. M. *Anal. Chem.* **2003**, *75*, 22-26.

(96) Kim, Y. D.; Park, C. B.; Clark, D. S. *Biotech. Bioeng.* **2001**, *73*, 331-337.

(97) Peterson, D. S.; Rohr, T.; Svec, F.; Frechet, J. M. J. *Anal. Chem.* **2002**, *74*, 4081-4088.

(98) Seong, G. H.; Heo, J.; Crooks, R. M. *Anal. Chem.* **2003**, *75*, 3161-3167.

(99) Seong, G. H.; Crooks, R. M. *J. Am. Chem. Soc.* **2002**, *124*, 13360-13361.

(100) Shimoboji, T.; Larenas, E.; Fowler, T.; Kulkarni, S.; Hoffman, A. S.; Stayton, P. S. *Proc. Natl. Acad. Sci. USA* **2002**, *99*, 16592-16596.

(101) Holden, M. A.; Cremer, P. S. *J. Am. Chem. Soc.* **2003**, *125*, 8074-8075.

(102) Green, R. J.; Davies, M. C.; Roberts, C. J.; Tendler, S. J. B. *Biomaterials* **1999**, *20*, 385-391.

(103) In a separate experiment, polyelectrolytes were adsorbed in PDMS/glass microchannels and photopatterned with B4F. Poly(diallyldimethyl ammonium chloride), poly(styrene sulfonic acid) polyacrylic acid and polyethylenimine (the only polymer with primary amine substituents) were used. Only the last species gave rise to a visible pattern when labeled streptavidin was introduced. All surfaces suffered from nonspecific adsorption.

(104) Kim, E. E.; Wyckoff, H. W. *J. Mol. Biol.* **1991**, *218*, 449-464.

(105) Amplex Red can spontaneously oxidize to the fluorescent product, resorufin; however, we found that the substrate used for HRPLS had little if any background fluorescence when introduced into a microchannel with no enzyme. Therefore, we attribute all pre-patch fluorescence to nonspecifically adsorbed enzyme.

(106) Bernard, A.; Michel, B.; Delamarche, E. *Anal. Chem.* **2001**, *73*, 8-12.

(107) Delamarche, E.; Bernard, A.; Schmid, H.; Bietsch, A.; Michel, B.; Biebuyck, H. *J. Am. Chem. Soc.* **1998**, *120*, 500-508.

(108) Groves, J. T.; Boxer, S. G. *Acc. Chem. Res.* **2002**, *35*, 149-157.

(109) Sackmann, E. *Science* **1996**, *271*, 43-48.

(110) Cremer, P. S.; Yang, T. L. *J. Am. Chem. Soc.* **1999**, *121*, 8130-8131.

(111) McConnell, H. M.; Watts, T. H.; Weis, R. M.; Brian, A. A. *Biochim. Biophys. Acta* **1986**, *864*, 95-106.

(112) Kam, L.; Boxer, S. G. *Langmuir* **2003**, *19*, 1624-1631.

(113) Groves, J. T.; Wulfing, C.; Boxer, S. G. *Biophys. J.* **1996**, *71*, 2716-2723.

(114) Groves, J. T.; Boxer, S. G. *Biophys. J.* **1995**, *69*, 1972-1975.

(115) Cremer, P. S.; Groves, J. T.; Kung, L. A.; Boxer, S. G. *Langmuir* **1999**, *15*, 3893-3896.

(116) Heldin, C. H. *Cell* **1995**, *80*, 213-223.

(117) Lees, W. J.; Spaltenstein, A.; Kingerywood, J. E.; Whitesides, G. M. *J. Med. Chem.* **1994**, *37*, 3419-3433.

(118) Mammen, M.; Choi, S. K.; Whitesides, G. M. *Angew. Chem. Int. Ed.* **1998**, *37*, 2755-2794.

(119) Lieto, A. M.; Cush, R. C.; Thompson, N. L. *Biophys. J.* **2003**, *85*, 3294-3302.

(120) Yang, T. L.; Jung, S. Y.; Mao, H. B.; Cremer, P. S. *Anal. Chem.* **2001**, *73*, 165-169.

(121) Yang, T. L.; Baryshnikova, O. K.; Mao, H. B.; Holden, M. A.; Cremer, P. S. *J. Am. Chem. Soc.* **2003**, *125*, 4779-4784.

(122) Kiessling, L. L.; Pohl, N. L. *Chem. Biol.* **1996**, *3*, 71-77.

(123) Pisarchick, M. L.; Gesty, D.; Thompson, N. L. *Biophys. J.* **1992**, *63*, 215-223.

(124) Meuse, C. W.; Krueger, S.; Majkrzak, C. F.; Dura, J. A.; Fu, J.; Connor, J. T.; Plant, A. L. *Biophys. J.* **1998**, *74*, 1388-1398.

(125) Ross, E. E.; Spratt, T.; Liu, S. C.; Rozanski, L. J.; O'Brien, D. F.; Saavedra, S. S. *Langmuir* **2003**, *19*, 1766-1774.

(126) Ross, E. E.; Rozanski, L. J.; Spratt, T.; Liu, S. C.; O'Brien, D. F.; Saavedra, S. S. *Langmuir* **2003**, *19*, 1752-1765.

(127) Axelrod, D.; Koppel, D. E.; Schlessinger, J.; Elson, E.; Webb, W. W. *Biophys. J.* **1976**, *16*, 1055-1069.

(128) Brown, E. B.; Wu, E. S.; Zipfel, W.; Webb, W. W. *Biophys. J.* **1999**, *77*, 2837-2849.

(129) Nollert, P.; Kiefer, H.; Jahnig, F. *Biophys. J.* **1995**, *69*, 1447-1455.

(130) Kalb, E.; Frey, S.; Tamm, L. K. *Biochim. Biophys. Acta* **1992**, *1103*, 307-316.

(131) Sackmann, E. *Febs Letters* **1994**, *346*, 3-16.

(132) Futai, M.; Tanaka, Y. *J. Bacteriol.* **1975**, *124*, 470-475.

(133) Owen, P.; Kaback, H. R. *Proc. Natl. Acad. Sci. USA* **1978**, *75*, 3148-3152.

(134) Altendor, K. H.; Staeheli, L. A. *J. Bacteriol.* **1974**, *117*, 888-899.

(135) Bayley, H.; Cremer, P. S. *Nature* **2001**, *413*, 226-230.

(136) Schuster, B.; Pum, D.; Braha, O.; Bayley, H.; Sleytr, U. B. *Biochim. Biophys. Acta* **1998**, *1370*, 280-288.

(137) Schuster, B.; Pum, D.; Sara, M.; Braha, O.; Bayley, H.; Sleytr, U. B. *Langmuir* **2001**, *17*, 499-503.

(138) Sleytr, U. B.; Bayley, H.; Sara, M.; Breitwieser, A.; Kupcu, S.; Mader, C.; Weigert, S.; Unger, F. M.; Messner, P.; JahnSchmid, B.; Schuster, B.; Pum, D.; Douglas, K.; Clark, N. A.; Moore, J. T.; Winningham, T. A.; Levy, S.; Frithsen, I.; Pankovc, J.; Beale, P.; Gillis, H. P.; Choutov, D. A.; Martin, K. P. *FEMS Microbiol. Rev.* **1997**, *20*, 151-175.

VITA

Matthew Alexander Holden

11348 Portside Drive
Jacksonville, FL 32225
Telephone: (904) 646-5895
E-mail: holden@mail.chem.tamu.edu

Education

May 04
Ph.D., Chemistry
Texas A&M University
Advisor: Dr. Paul Cremer
Research Areas: Microfluidics, Photopatterning, Artificial Bilayers

May 99
Bachelor of Science, Chemistry
University of Florida
Advisor: Dr. Richard Yost
Research Area: ESI-Ion Trap-MS of High Explosives

Research Publications

(1) Mao, H.; Holden, M. A.; Yu, M.; Cremer, P. S. *Anal. Chem.* **2002**, *74*, 5071-5075.

(2) Holden, M. A.; Kumar, S.; Castellana, E. T.; Beskok, A.; Cremer, P. S. *Sens. Actuators B* **2003**, *92*, 199-207.

(3) Holden, M. A.; Cremer, P. S. *J. Am. Chem. Soc.* **2003**, *125*, 8074-8075.

(4) Yang, T. L.; Baryshnikova, O. K.; Mao, H. B.; Holden, M. A.; Cremer, P. S. *J. Am. Chem. Soc.* **2003**, *125*, 4779-4784.

(5) Holden, M. A.; Kumar, S.; Beskok, A.; Cremer, P. S. *J. Micromech. Microeng.* **2003**, *13*, 412-418.

(6) Holden, M. A.; Jung, S. Y.; Cremer, P. *Anal. Chem.* **2004**, *in press*.